INSTITUTE FOR DEFENSE ANALYSES

Risk of Auditory Injury Caused by Area-Effect Flashbangs: Multiple Area-Distributed Impulses and the Role of the Acoustic Reflex

Jessica G. Swallow
Emily A. Fedele
Felicia D. Sallis-Peterson

March 2021

Approved for public release;
distribution is unlimited.

IDA Document D-21609

Log: H 21-000099

INSTITUTE FOR DEFENSE ANALYSES
4850 Mark Center Drive
Alexandria, Virginia 22311-1882

The Institute for Defense Analyses is a nonprofit corporation that operates three Federally Funded Research and Development Centers. Its mission is to answer the most challenging U.S. security and science policy questions with objective analysis, leveraging extraordinary scientific, technical, and analytic expertise.

About This Publication

This work was conducted by the IDA Systems and Analyses Center under contract HQ0034-19-D-0001, Project DU-2-4640, "Auditory Impulse Modeling Assessment," for the Joint Nonlethal Weapons Directorate (JNLWD) and the Joint Intermediate Force Capabilities Office (JIFCO). The views, opinions, and findings should not be construed as representing the official position of either the Department of Defense or the sponsoring organization.

For More Information

Jessica G. Swallow, Project Leader
jswallow@ida.org, (703) 845-2490

Leonard J. Buckley, Director, Science and Technology Division
lbuckley@ida.org, (703) 578-2800

Copyright Notice

© 2021 Institute for Defense Analyses
4850 Mark Center Drive, Alexandria, Virginia 22311-1882 • (703) 845-2000.

This material may be reproduced by or for the U.S. Government pursuant to the copyright license under the clause at DFARS 252.227-7013 (Feb. 2014).

INSTITUTE FOR DEFENSE ANALYSES

IDA Document D-21609

Risk of Auditory Injury Caused by Area-Effect Flashbangs: Multiple Area-Distributed Impulses and the Role of the Acoustic Reflex

Jessica G. Swallow
Emily A. Fedele
Felicia D. Sallis-Peterson

Executive Summary

Background

Flashbang devices are intermediate force capabilities that are designed to produce sound and light effects that can startle or disorient exposed individuals. Although they are not intended to produce permanent injuries, these devices do have the potential to cause hearing loss (permanent threshold shift, or PTS), along with other injuries. Because of this potential, a model known as Auditory 4.5 was developed by L3 Applied Technologies with support from the Department of Defense's Joint Intermediate Force Capabilities Office (JIFCO) for estimating the risk of PTS from impulse-noise exposures. This model can account for variation in angle of incidence from sound to target's ears, but has limited capability to account for multi-impulse, area-distributed exposures, particularly those that deliver impulses of varying intensity in short time frames. Although multi-impulse flashbangs are actively of interest for use in military operations, the role of design variables such as the number of impulses, the distribution of impulses (i.e., some devices use a single projectile that subsequently disperses multiple "submunitions" across an area, each of which delivers an impulse, resulting in area-distributed impulses), or the uncertainty in device output in computing overall injury risk is not well explored.

Furthermore, the injury risk associated with multi-impulse exposure in short time frames is linked to two key human effects that are difficult to model: (1) temporary changes in the mechanical properties of tissues in the auditory system, particularly the tympanic membrane, after blast exposure, and (2) temporary contraction of muscles in the middle ear known as the acoustic reflex. These effects may influence overall risk of injury in competing ways.

Our main goal in this report is to demonstrate bounded injury-risk estimation for multiple-impulse, area-distributed flashbang exposures in the acoustic reflex regime. We also analyze how variables in device design such as the number of impulses, the dispersion radius of submunitions, and the uncertainty in the submunition output sound intensity affect risk estimates. Our approach is designed to be broadly applicable to operational concepts in which impulses may be distributed over an area and readily extensible to understanding risk profiles for specific target distribution and device parameters. To illustrate our approach, we present analysis of a device design in which a single mortar projectile distributes multiple submunitions in an area. Within seconds of dispersal, each submunition releases an impulse of sufficient intensity to cause some risk of PTS. This design is similar to the design of the indirect fire munition (IDFM), which is currently

under development and has been proposed as a tool for suppressing individuals at range or moving individuals away from or denying them access to an area.

Our analysis makes use of the concept of the "dose-accumulation rule," a mathematical relationship used to estimate the aggregate injurious "dose" received by a target exposed to multiple hazardous stimuli of a similar type. Auditory 4.5 uses a dose of A-weighted sound exposure level, which weights the energy content of an impulse noise by the sensitivity of the human auditory system to different frequencies. It has been shown that the dose delivered by multiple impulses is not strictly additive; that is, the dose delivered by several impulses is typically less than the sum of the individual doses.

Methods

In this analysis, we apply limiting assumptions for dose-accumulation rules for PTS risk estimation from multi-impulse flashbangs. The lower bound risk was estimated by assuming a 100% protective acoustic reflex after the first impulse, while the upper bound risk was estimated by applying the equal energy criterion, which permits no trading for intensity vs. number of impulses in computing injury risk. The true injury risk is expected to lie between these extremes, as the equal energy criterion has been shown to overestimate risk for various types of impulse noise, and the acoustic reflex is known to be absent in a subset of the population. Using these limiting assumptions, and to account for the variability in risk caused by variation in submunition distribution, we conduct Monte Carlo simulations of submunition dispersion and timing of multi-impulse flashbangs. We generate maps of injury risk as a function of position in our simulated scene for different device parameters and dose-accumulation rules. The results of these simulations are used to explore tradeoffs between device design and risk and to understand how uncertainties in our estimates are related to these design parameters.

Results

The bounded injury-risk-estimation method worked as expected, with the intermediate estimate always below the upper bound and above the lower bound.

In general, risk maps generated in this study show an annular region of maximum risk in the simulated 25 × 25 m scene, with a maximum risk position close to the submunition dispersion radius of the mortar. This pattern is a consequence of the device design used in our analysis, which distributes submunitions according to a uniform distribution of angle at some distance from a fixed burst point, which designates the position at which the mortar round releases the submunitions. The resulting pattern of munitions is typically distributed in a ring shape, with few munitions near the burst point of the mortar round. The table below summarizes the effect of changing various parameters in the mortar device design on the peak risk as a function of radial position relative to the burst point and scene-averaged risk for the 25 × 25 m simulations conducted in this study.

Summary of Effects on Peak and Scene-Averaged RSI of Varying Parameters in Design of a Mortar Device that Distributes Submunition Flashbangs over an Area

Action	Effect on Peak Risk	Effect on Scene-Average Risk
Increase burst radius R	Decrease (moderate)	Non-monotonic, depends on scene size
Increase burst radius uncertainty σ_r	Decrease (minor)	Increase (minor)
Increase average inter-pulse interval λ	Decrease (minor)	Decrease (minor)
Increase number of submunitions N_b	Increase (major)	Increase (major)
Increase average pulse intensity $\bar{f}$	Increase (major)	Increase (major)
Increase standard deviation of pulse intensity σ_f	Increase (moderate)	Increase (moderate)

We note that distributing submunitions over a wider area has the effect of reducing the expected peak risk in the area while spreading risk more evenly. Because of the asymmetry in the logistic injury-risk curve contained in Auditory 4.5, in the typical flashbang dose regime, small increases in device output (in dBA) have a greater impact on risk than small decreases. For the same reason, increased device output variance, although with equal ±dB values, has the effect of increased expected and peak injury risk in the scene. These results illustrate the need for aggregate RSI calculations to factor in device output variation, and not simply compute risk based on the mean or expected device output.

Both the computed risk and the range of uncertainty due to the dose-accumulation rule more than double when the threshold of significance for PTS is dropped from 40 to 25 dB. The asymmetry of the logistic-regression curve in the flashbang dose regime is slightly reduced as well for this change. The difference of 15 dB in the threshold of significant injury makes a substantial impact on risk estimates. These thresholds should be carefully considered when trying to understand the human effects of flashbangs.

Our results point to choices that may be available in the design of a submunition-dispersing flashbang mortar to tune injury-risk profiles. For example, if the designer's goal is to reduce overall *average risk* in an area, changes such as decreasing the uncertainty in individual impulse-output intensity may be appropriate, in addition to more obvious actions such as decreasing the number of submunitions or the expected sound output intensity of individual submunitions. In contrast, to decrease the *peak risk* in an area, actions such as increasing the radius of submunition dispersion or the uncertainty of the submunition dispersion radius or decreasing the individual impulse-intensity uncertainty may be appropriate.

Our analysis also demonstrated that the uncertainty in the dose-accumulation rule can lead to large uncertainties in expected RSI, particularly when the number of impulses is high or the overall risk of injury is high. The pattern of submunitions in these simulations generates uncertainty in the estimated RSI throughout an area; we found that the sizes of these uncertainty ranges expressed as a proportion of peak risk *decreased* with an increased number of submunitions. Furthermore, the risks computed in the highest risk region of the exposure scene were more sensitive to the pattern of submunitions than those computed in the low-risk regions of the scene.

In contrast, the dose-accumulation rule RSI uncertainty ranges expressed as a proportion of peak risk increased with the number of submunitions. These uncertainty ranges are representative of our uncertainty about risk in the acoustic-reflex (less than 1 s inter-pulse interval) regime. Overall, our analysis shows that uncertainty about the role of the acoustic reflex in protecting targets from significant injury becomes more important when multi-impulse tactics and devices are employed in short (sub-second) time intervals.

This work provides a methodology for exploring both the role of device parameters and the choice of dose-accumulation rule in estimating RSI and associated uncertainty for multi-impulse, area-distributed exposures with short (<1 s) inter-pulse intervals. This analysis can describe how decisions about the design and operational usage of flashbangs (e.g., number of devices used and aim points) affect potential risk patterns in an area, as well as the uncertainty associated with those patterns. To make full use of this analysis, similar work exploring the influence of such parameters on the human effectiveness of devices is also required. Ultimately, devices are intended to have low RSI while retaining high human effectiveness. This can be a challenging balance to achieve with flashbangs, and the optimal selection of device parameters may vary, depending on the operational context (indoor, outdoor, day, night, etc.) in which devices are deployed.

Contents

1. Introduction

Modeling of the human effects of intermediate force capabilities (IFCs) is a critical step in the design, acquisition, and application of such devices for military purposes. In particular, IFCs, also known as non-lethal or less lethal weapons, are intended to be *effective* (able to achieve actions such as warning or dispersing individuals, denying access to an area, or delaying, channeling, or suppressing hostile actors) while minimizing *risk of significant injury* (RSI) to personnel or irreversible damage to infrastructure or materiel. *Significant injury* is defined by Department of Defense regulations (DoD 2013) as injury that will result in lifelong restriction on a person's activities or death if medical aid beyond limited first-responder care is not received. Accurate modeling of RSI is essential to providing commanders, warfighters, and weapon developers with an appropriate understanding of the likely outcomes of using IFCs. Such information can then be used to guide use-of-force decisions and design training requirements for using IFCs.

For many IFCs, it is difficult to model the range of variation that may occur in an operational setting. The nature of the surrounding environment (e.g., urban, natural, indoor, outdoor, daylight, night), the target distribution and disposition (e.g., intentions, hostility, awareness), and the weapon settings (e.g., aim point) produce an enormous variable space that may not be replicated in a laboratory setting. Computational modeling is typically the only available means to bridge the gaps between available experimental data and actual usage scenario variability.

Flashbangs are a particularly interesting example of the gaps that exist between operational variability and injury-risk prediction. Flashbangs are IFCs designed to produce sound and light effects that can startle, acutely stress, or disorient exposed individuals. Although they are not intended to produce permanent injuries, because of the intensity of sound produced by these devices (typically 170–180 dB[1] at a distance of 5–6 feet) the potential for certain types of auditory injury exists from flashbang exposure, including hearing loss (permanent threshold shift, or PTS) (Swallow and Sallis-Peterson 2020). Because of this potential, a model known as Auditory 4.5 was developed by L3 Applied Technologies with support from the Department of Defense's Joint Intermediate Force Capabilities Office (JIFCO) for estimating the risk of hearing loss from impulse-noise

[1] Peak sound pressure levels, or SPL, can be expressed in units of decibel (dB), which is defined as $20*\log_{10}(P/P_0)$, where P is the maximum sound overpressure and P_0 is the reference pressure of 20 μPa. Flashbang impulses include very high overpressures that can injure the auditory system, for example by rupturing the tympanic membrane, along with other human effects not covered in this report.

exposures. This model can account for variation in angle of incidence from sound to the target's ear, but has limited capability to account for multi-impulse exposures of varying individual-impulse intensity (such as those from the indirect fire munition, or IDFM), particularly in short time frames. Furthermore, the model does not have any built-in features to account for other kinds of operational uncertainties, including the absorptive or reflective characteristics of surrounding environments, weapon aiming and dispersion, and the number, positioning, or behavior of targets. Although considering all these factors was beyond the intended scope of the initial model development, they will influence how the outputs (sound and light) of a given flashbang are perceived by a target and the resulting injury risk and human effectiveness.

In this report, we will discuss and explore several key issues:

- Quantification of uncertainty in injury-risk estimation related to exposure to multiple area-distributed flashbang impulses in short periods of time.
- Analysis of the effects of factors such as the number of impulses, their spatial distribution, their timing, and the uncertainties in their parameters (e.g., impulse intensity) on injury risk and estimates of injury risk.
- Analysis of how the choice of threshold for significant injury affects overall risk.

A. Multi-impulse Exposures and the Acoustic Reflex

The characterization of multiple-impulse, area-distributed flashbang exposure is of particular importance because such systems are actively being designed for military use (JNLWP 2015). In particular, the IDFM is intended to be a mortar system that would disperse several submunitions that would then detonate over an area within a short time frame (on the order of seconds) (JNLWP 2015).[2] This type of device is intended to enable non-lethal effects at range, such as suppressing individuals in an area, moving individuals away from an area, or denying them access to an area. This report focuses on the area-effects of this device, accounting for the randomness in where submunitions land. This analysis is distinct from analysis of individual impulse devices, which would typically focus on risk as a function of distance from the device detonation point.

The injury risk associated with multiple-impulse exposure in short time frames is linked to two key human effects that are difficult to model: (1) temporary changes in the

[2] Although flashbangs may be used in conjunction with other impulse-noise-generating devices (i.e., rifles), this report is focused on estimating RSI for multi-impulse flashbangs alone. RSI, which is used to quantify risks to targets from non-lethal weapons, is typically not quantified for lethal weapons or operator use. Risks to the soldiers deploying flashbangs, including in combination with other devices, would fall under the category of occupational hazard assessments.

mechanical properties of tissues in the auditory system, particularly the tympanic membrane (i.e., the eardrum), that occur immediately following impulse exposure and (2) temporary contraction of muscles in the middle ear, known as the acoustic reflex.

Exposure to impulse noise can change the properties of the tympanic membrane (TM), at least temporarily[3] (Liang et al. 2017, 2016; Engles, Wang, and Gan 2017; Liang et al. 2019). After only a few blast exposures, both human and chinchilla tympanic membranes have been shown to exhibit decreased stiffness, and chinchilla tympanic membranes have also been shown to exhibit decreased failure pressure.[4] The duration of the effect is unclear—these studies were conducted on ex situ specimens or specimens harvested immediately after blast; therefore, recovery and healing mechanisms that may be active in vivo were not possible to trace. Moreover, it is unclear if repeated sub-injurious blasts will continually degrade mechanical properties, such as the stiffness of the membrane, or if there is some asymptotic effect. Regardless, a loss of stiffness in the TM should affect the efficiency of sound coupling to the cochlea (i.e., the part of the inner ear that receives the sound vibrations from the TM and converts these into nerve impulses for the brain), likely in a frequency-dependent way. Such changes should therefore affect the risk of hearing loss, although the magnitude of that effect is unknown. In terms of computing injury risk from repeated auditory blasts in short time frames, this effect of mechanical property degradation might contribute to an increased injury risk relative to longer time frames over which healing can be expected to occur.

Another physiological effect that is at play with repeated auditory blasts is the acoustic reflex, a contraction of muscles in the middle ear that causes a change in the impedance of the tympanic membrane, altering the efficiency of sound transmission to the cochlea. Although often triggered by intense noise exposure, it can be caused by other events such as quick eye movements (Gruters et al. 2018). The characteristics of the acoustic reflex, including the time to activation, the duration of effect, the general shape of the response profile, and the intensity, are highly variable across subjects and elicitor stimuli, making modeling of this effect difficult (Jones, Greene, and Ahroon 2019;

---

[3] Specimens in these experiments were harvested and their mechanical properties measured within minutes to hours of blast exposure. Because specimens were either post-mortem or harvested, the potential recovery effects of healing were not captured by these experiments.

[4] Stiffness describes resistance to elastic (reversible) deformation when subjected to mechanical stress. Changes in tympanic membrane stiffness affect the efficiency with which sound is transmitted to the middle ear. Decreased stiffness causes membranes to undergo larger strains for the same stress load, which can cause failure at lower stress if failure is strain-limited. Failure pressure is the required applied pressure to rupture the membrane. After exposing anesthetized chinchillas to three intense overpressure impulses (“blasts”) generated by pressure-driven rupture of polycarbonate films, Liang et al. (2017) harvested the chinchilla bulla, measured tympanic membrane viscoelastic properties, and then gradually applied air pressure to the tympanic membranes of chinchilla subjects until rupture occurred. This defined failure pressure in their experiments.

McGregor et al. 2018; Church and Cudahy 1984; Durrant and Shallop 1969; Deiters et al. 2019).

Several studies have suggested that the reflex could reduce the risk of hearing loss (Dancer et al. 1991; Fletcher and Riopelle 1960; M. Loeb, Fletcher, and Benson 1965; Danielson et al. 1991). For example, Dancer et al. (1991) found that the degree of temporary hearing loss of soldiers exposed to rifle fire was reduced when shots were fired in burst mode (60 ms inter-pulse-interval) relative to when shots were fired in longer (10 s) intervals. The hypothesis of these studies was that the reflex could engage over short time frames (about 60–200 ms) following an impulse and that this was a protective reflex that decreased temporary threshold shift (TTS) for short inter-pulse-interval exposures, potentially also decreasing permanent injury risk. The reflex has been estimated to remain fully active for between 40 and 600 ms following activation, depending on the stimulus (Church and Cudahy 1984; Dallos 1964; Jones, Greene, and Ahroon 2018) and to undergo a gradual deactivation that can take up to a second (Church and Cudahy 1984).

The acoustic reflex is common in the human population, but not pervasive (Flamme et al. 2017; McGregor et al. 2018). A study of over 15,000 health records for individuals aged 12 and over found that approximately 75% of subjects exhibited the acoustic reflex in at least one ear during pure tone stimulation at 105 dB SPL, and about 52% exhibited the reflex in both ears (Flamme et al. 2017). These proportions increased to 85% and 68%, respectively, for subjects aged 18–30. An additional study using a diagnostic middle ear analyzer detected an acoustic reflex in both ears for approximately 92% of participants; however, this study pulled from a population with particularly strong hearing (McGregor et al. 2018). Another study exposed 190 subjects to short-duration elicitor sounds (e.g., recordings of rifle shots, 100 ms pure tone signals) scaled to a 100 dBA sound exposure level (Deiters et al. 2019). The acoustic reflex was observed in 15%–70% of subjects, depending on the elicitor, with rifle sounds (most similar to flashbangs) producing reflex responses in less than 50% of participants. These studies suggest that impulse noise can elicit the acoustic reflex, but not reliably. However, these studies had to limit the intensities of exposures to prevent injury to participants—it is possible that more intense impulse noise more representative of flashbang exposure could elicit the reflex in a larger proportion of subjects.

The studies described above have concluded that when determining damage risk criteria for occupational health hazard assessments, it is not appropriate to assume that subjects have an active acoustic reflex. In the occupational health context, standards are typically defined to protect at least 95% of people (Flamme et al. 2017). In contrast, injury risk assessments for IFCs for military use seek to quantify risks to targets, rather than set safety standards, because such devices are often used as an intermediate step in escalation of force during combat operations. In that context, and depending on the engagement, a moderate risk of injury may be acceptable to the commander if the alternative is to use a

lethal weapon. Therefore, when computing risk of injury from IFCs, we should try to account for the acoustic reflex to get a more accurate assessment of the risk to the exposed population.

B. Auditory 4.5

1. Background

Experimental data on the human effects, and particularly the injury risks, of IFCs are often very difficult to obtain. As a result animal data or post-mortem human subject (PMHS) data are used to try to understand injury risks associated with various devices. Often, data on occupational exposures to related hazards are used to supplement such sources. One example of this type of data aggregation is the model currently provided by JIFCO for estimating risk of hearing loss (PTS and temporary threshold shift, TTS) due to impulse noise exposure: Auditory 4.5.

Auditory 4.5 uses sound recordings as inputs and produces estimates of injury risk (TTS at 2 minutes post exposure or PTS) as outputs (P. Chan, Ho, and Ryan 2016; P. Chan, Ho, and Zagadou 2018). Auditory 4.5 is an empirical model that was built by using a mix of animal (chinchilla) exposure data and occupational (human) rifle-noise exposure data. PTS and TTS cannot be measured post-mortem, so no PMHS data were used to build Auditory 4.5's injury risk dose-response curves. Auditory 4.5 computes risk of injury (i.e., PTS) according to a logistic regression with coefficients b_0 and b_1 dependent on the threshold of interest K (Equations 1–3):

$$P(\text{Threshold Shift} \geq K \text{ dB}) = \frac{e^L}{1+e^L} \tag{1}$$

$$L = b_0 + b_1 A \tag{2}$$

$$A = SELA \text{ in dB} + B - C - D \tag{3}$$

The dose A is the A-weighted sound exposure level (SELA) computed for a single impulse, with additional correction for dose accumulation (*B;* see below), scaling from chinchilla subjects to human subjects (C = 28 dB), and angle of incidence (D, determined based on a lookup table that accounts for attenuation of sound that may occur due to diffraction around the head (P. Chan, Ho, and Zagadou 2018)). The dose-accumulation formula used in Auditory 4.5 is given by Equations 4–5:

$$B = 3.44 \log_{10} N \,, N < 25 \tag{4}$$

$$B = 3.44 \log_{10} N/25 + 3.44 \log_{10} 25 \,, N \geq 25 \tag{5}$$

Equations 4 and 5 add a correction factor to the computed SELA of a single impulse to estimate the effective dose for multiple identical impulses. Note that Equation (4) suggests that dose accumulation is attenuated for less than 25 impulses; that is, the dose resulting from 10 equivalent impulses delivered at least 1 second apart is equal to the dose from a single impulse with 3.44 times the A-weighted energy. This is called an N-trading rule and was developed based on analysis of data from human blast exposure with hearing protection (P. C. Chan et al. 2001).

Because the data used to build Auditory 4.5 used inter-pulse intervals (IPIs) of at least 1 second for identical impulse stimuli, Auditory 4.5 has not been calibrated for exposures that might involve the acoustic reflex or exposures with multiple impulses of varying intensity. In this analysis, we explore how to bound injury risk estimates based on Auditory 4.5 by applying limiting assumptions for dose-accumulation rules applied to short IPIs and varied impulse-noise-intensity exposures characteristic of devices such as multi-impulse flashbangs.

2. Limiting Assumptions on Dose Accumulation

A dose-accumulation rule is a mathematical relationship used to estimate the aggregate injurious "dose" received by a target exposed to multiple hazardous stimuli of a similar type. N-trading rules, which have been widely used to account for dose accumulation in impulse-noise-injury risk estimation (Smoorenburg 2003), can be formulated according to Equation 6:

$$\mathrm{Dose}(N) = SELA(\text{single impulse}) + 10\chi \log_{10} N \tag{6}$$

The value of the coefficient χ (0.344 for Auditory 4.5's existing rule) varies for different noise sources (Smoorenburg 2003). For example, data for spark-gap exposures (Michel Loeb and Fletcher 1968) suggest χ = 0.83, data for blast-overpressure exposures (Patterson et al. 1997) suggest χ is between 0.2 and 0.35, and data from rifle-noise exposures (Coles et al. 1967; Pfander et al. 1980; Dancer et al. 1991) place χ between 0.1 and 0.72 for few (less than 50) and for many (more than 50) impulses, respectively. An equal-energy criterion (which computes the dose based on total energy delivered and therefore assumes no trading for multiple impulses) corresponds to χ = 1.

Wang, Burgei, and Zhou (2017) derived a more generalized form of these N-trading rules analytically based on a framework of "immunity." In their work, Wang, Burgei, and Zhou postulated an "immunity factor" to account for the reduced apparent injury risk of multiple impulses relative to single impulses delivering equivalent energy. With this parameter, they derived Equation 7, which computes an effective composite dose G_{eff} for multiple impulses of unequal intensities, using the parameter χ to account for the strength of this immunity factor:

$$G_{\text{eff}} = A_{i,\max} + 10\chi \log_{10} \sum_{i=1}^{N} 10^{\frac{A_i - A_{i,\max}}{10\chi}} \; (0 \le \chi \le 1) \tag{7}$$

In Equation 7, $A_{i,\max}$ is the maximum value in the set $\{A_i\}$, where the $\{A_i\}$ are computed for each individual impulse in the series and incorporating corresponding angle-of-incidence corrections $\{D_j\}$ according to Equation 8:

$$A_{\text{i}} = SELA_{\text{i}} - D_i \; (0 \le \chi \le 1) \tag{8}$$

For input to Auditory 4.5, this G_{eff} is then combined with the human-chinchilla scaling correction C following Equation 9 to form an effective dose A_{eff} that replaces A in Equation 2:

$$A_{\text{eff}} = G_{\text{eff}} - C \tag{9}$$

Equation 7 was derived analytically from Equation 4 and the definition of A-weighted sound exposure level SELA. It does not include mechanistic justification for the value of χ, but including this parameter gives the analyst flexibility about the assumptions being made. Setting $\chi = 1$, as we have stated, assumes an equal-energy criterion. This should be considered as an upper bound for estimating the effective dose of a multi-impulse exposure, because experimental data have found values of χ that are consistently less than 1. On the other hand, setting $\chi = 0$ effectively sets the dose equal to the dose of the most severe impulse. Intermediate values of χ can be used to tune dose-accumulation rules to be more representative of different types of impulses, such as spark gaps, rifle noise, and blast.

On the other hand, we can apply a lower bound on dose-accumulation by assuming that a target's acoustic reflex engages immediately following the first impulse the target hears and that until the reflex relaxes, the target is completely protected from additional impulses (even if they are louder). In this case our dose-accumulation rule follows Equation 10:

$$A_{\text{eff}} = A_{\text{first pulse}} \tag{10}$$

Here, $A_{\text{first pulse}}$ is computed following Equation (3) with $N = 1$ ($B = 0$). Based on review of literature on the acoustic reflex, the risk of injury computed with dose determined via Equation 10 for multi-impulse scenarios should be an underestimate of the expected value. Not only does a significant proportion of the population have a weak or non-existent acoustic reflex, but the reflex does not remain at full strength indefinitely. Even when the reflex is at full strength, there is little evidence that it would completely prevent additional risk of hearing loss with additional impulse exposures. However, there is always the potential of a target taking protective actions, such as covering the ears, immediately after a first impulse is heard. Equation 10 is therefore still a reasonable choice of lower bound on dose estimation.

Combining these assumptions, we can bound the estimation of dose for complex multi-impulse exposures to flashbangs: on the upper bound, we assume the equal energy criterion (Equation 7 with $\chi = 1$), and on the lower bound, we assume a perfect acoustic reflex (Equation 10). The true effective dose within the Auditory 4.5 logistic-regression injury-risk model framework should sit between these extremes, with χ chosen to represent the type of impulse that is of interest. For the analysis in this report, we use Equation 7 with $\chi = 0.344$ to represent a best guess for multi-impulse flashbang exposures, because this is the value that is most consistent with the existing Auditory 4.5 model.

C. Objective

1. Background

Our goal is to demonstrate bounded injury-risk estimation for PTS from multi-impulse flashbang exposures that may trigger the acoustic reflex and to explore how design variables in devices that distribute multiple flashbang submunitions over an area affect the range of injury risk determined. Our analysis draws upon the work of Wang, Burgei, and Zhou (2018) investigating the risk of hearing loss injury for multiple flashbangs in a crowd. In that work, the authors applied a probabilistic modeling approach to simulating flashbang submunition dispersal over an area and computed injury risk contour maps using a fixed dose-accumulation rule (Equation 7 with $\chi = 0.344$), but varying factors like aiming error and number of subjects. The authors made use of experimental flashbang recordings to estimate the SELA in decibels as a function of distance from the device ρ (in meters). We will re-use their Model B derived from that experimental data, which is given by Equation 11:

$$SELA(\rho) = -20\log_{10}(\rho) - 0.5\rho + 148.5 \tag{11}$$

Our goal in this analysis is to demonstrate bounded injury-risk estimation for multiple-impulse flashbang exposures, accounting for the possible effects of the acoustic reflex. We focus on how variables in flashbang design affect these risk bounds, such as the number of impulses, the dispersion radius of the submunitions, and the uncertainty in the submunition output sound intensity or timing. Our analysis builds on the work of Wang, Burgei, and Zhou, adding in complexity with angle-of-incidence correction, aggregating risk across two ears at each target position, and considering the role of timing in the exposure. Specifically, by including timing parameters in our probabilistic simulation, we are able to combine the energy of impulses that occur close together in time, representing the idea that in very short time frames (<50 ms), the ear may not distinguish between multiple impulses. Our approach is designed to be broadly applicable to devices of this type and readily extensible to understanding risk profiles for specific target distribution and device parameters.

2. Aggregating Risk

An additional complexity arises in our analysis from the need to account for a subject's two ears. The Auditory 4.5 model is best understood to estimate the risk of injury to a single ear exposed to the sound input to the model. That is, the large source data set that the model was built from used monaural animal subjects, and much of the human rifle noise data used to calibrate the model to humans also reported the proportion of injury on a basis of number of ears, rather than on the number of subjects. When computing risk of injury to a *subject*, however, we must compute the risk of injury to *at least one ear*, rather than the risk of injury to a single ear.

Considering the full population of potential targets, there are some variables (e.g., subject age or past exposure history) that could cause correlation in the injury susceptibility of the two ears of a subject.[5] While some correlation between right and left ear risk in individuals may exist, there are not sufficient data available to estimate that correlation. Similarly, data are lacking for applying adjustments for two-ear injury-risk correlation based on subject age or history.

Given that Auditory 4.5 was built on data for which right and left ears were not distinguished or for which only one ear was available per subject, any correlation that may have existed in the injury outcomes for subjects' two ears was lost in the model-building process. The simplest option is therefore to treat ears independently for the purpose of estimating risk to a subject. In other words, we assume that the outcome to one ear does not affect the risk of injury to the other ear and compute risk of injury to a subject following Equation 12:

$$\text{Risk(Subject)} = \text{Risk(Ear } A) + \text{Risk (Ear } B) - \text{Risk(Ear } A) * \text{Risk(Ear } B) \quad (12)$$

This is expected to lead to some overestimates of injury risk. However, without data that distinguish between individual ear and individual subject risk, we do not have enough information to quantify this error. Since typical exposures will produce unequal doses to the left and right ears (due to angle-of-incidence effects), this error is expected to be small relative to real differences in injury risk to the ears caused by differing exposures. Equation 12 computes the risk to individual ears using the appropriate angle corrections for each ear, allowing us to account for this effect.

---

[5] For example, data suggest that the stiffness of the middle ear decreases with age, potentially changing the damage risk associated with a given input sound (Feeney and Sanford 2004). A number of studies have also found that the left ear is more susceptible to hearing loss than the right ear (Le et al. 2017; Munjal and Singh 1997; Cox and Ford 1995; Nageris et al. 2007). However, asymmetric hearing loss has typically been detected for long-term occupational exposures, rather than single traumatic exposures of similar magnitude for both ears, making it difficult to link these results to injury-risk prediction for flashbangs.

Note also that the problem of aggregating risk is a common issue in non-lethal weapon injury-risk modeling, especially when multiple modes of injury are possible (e.g., auditory injuries, eye injuries, blunt-impact injuries, etc.). It is not always the best choice to assume independence of different injury modes because there may be correlating variables that either increase or decrease the risk of additional injuries, depending on the outcome for one injury mode. A mild (not significant) injury of one type may increase the likelihood of a significant injury of another type. When computing RSI, dependencies among different injury routes should be incorporated whenever possible, especially when certain types of injury are easier to model than others.

2. Methods

In our bounding analysis for a multi-impulse flashbang, we are interested in understanding the effect of a number of parameters on RSI. Due to the variation in parameter estimates, we conducted Monte Carlo simulations of dispersion and timing of flashbangs distributed over an area following an approach similar to that used by Wang, Burgei, and Zhou (2018). The simulation used the following algorithm to generate maps of injury risk as a function of position for different device parameters (with reference to Figure 1, which appears after the steps):

1. Start with a grid centered at the burst point of the mortar, designated (0, 0). Assume targets all face in the +y direction (right and left ears oriented on *x*-axis). Assume all targets have a height *h* of 1.7 m.
2. For the N_b submunitions contained in the mortar, draw detonation characteristics $\{r_i, \theta_i, t_i, f_i\}$:
    a. *r* represents the radius from the burst point (positioned at 0, 0 in the grid) to the detonation point of the submunition and is drawn from a normal distribution with mean *R* and standard deviation σ_r.
    b. θ is drawn from a uniform distribution [0, 2π].
    c. The timing of impulse *i* is given by $t_i = t_{i-1} + \Delta t_i$ where Δt_i is the inter-pulse-interval, or IPI, drawn from an exponential distribution with parameter λ. The first impulse is set to occur at time 0. Most often, λ is set to 1/150 ms.
    d. *f* is a random ±dB added to each impulse SELA as computed from Equation 11, representing uncertainty in the output intensity from the submunition. *f* is drawn from a normal distribution with center $\bar{f}$ and standard deviation σ_f. Most often, $\bar{f}$ is set to 0. In some simulations, $\bar{f}$ was set to a non-zero value to add a consistent bias to the impulse output intensity over the SELA computed from Equation 11.
    e. *r* and θ are relative to grid origin (0, 0), which represents the burst point of the mortar device. One can directly compute the (*x*, *y*) position of each submunition from (r, θ) through simple coordinate transforms. Note that in operational scenarios, the *burst point* of the mortar (the point from which submunitions are dispersed) may deviate slightly from the *aim point* due to aiming error. In this report, all analysis is conducted relative to the *burst point*.

3. For each of the 625 points *j* in the exposure grid and each submunition *i*:

   a. Compute the distance ρ_{ij} from the grid point to the detonation point, accounting for subject height:

$$\rho_{ij} = \sqrt{(x_i - x_j)^2 + (y_i - y_j)^2 + h^2} \tag{13}$$

   b. Compute the yaw angle for each ear from that point to the detonation point

$$\alpha_{ij} = \cos^{-1} \frac{y_i - y_j}{\sqrt{(x_i - x_j)^2 + (y_i - y_j)^2}} \tag{14}$$

   The two ears will have yaw angles α_{ij} and $2\pi - \alpha_{ij}$. Yaw is the horizontal component of the angle of incidence, as shown schematically in (P. Chan, Ho, and Zagadou 2018).

   c. Compute the pitch angle β_{ij} from the point to the detonation point:

$$\beta_{ij} = -\rho_{ij} \sin^{-1} \frac{h}{\rho_{ij}} \tag{15}$$

   Pitch is the vertical component of angle of incidence and is determined relative to the horizontal plane that intersects the subject's ears.

   d. Determine resulting SELA based on f_i, angle corrections based on the pitch and yaw lookup tables (P. Chan, Ho, and Zagadou 2018), and distance from detonation point ρ_{ij} (use Equation 11). Because the lookup table does not cover the full 180° of pitch, the angle correction *D* for pitch between –60° and –90° is set equal to the angle correction for pitch equal to –60°.

   e. Compute the effective time of detonation perceived at the grid point *j*, T_{ij}, by adding the travel time from detonation point to grid point (ρ_{ij} /343 m/s, where 343 m/s is the speed of sound at sea level at 20 °C) to t_i.

   f. If any pairs of consecutive impulses now have $\Delta T = T_{ij} - T_{(i-1)j} \leq \tau = 50$ ms, these impulse pairs are combined into one impulse using the equal energy rule (Equation 7 with $\chi = 1$). This is done recursively until the resulting pulse train for grid point *j* contains no ΔT values below the threshold τ.

4. For each point in the grid, sum the set of SELAs according to three rules:

   a. The lower bound (perfect acoustic reflex)—Equation (10).

   b. The best guess (Wang, Burgei, and Zhou 2018 derivation based on Auditory 4.5)—Equation 7 with $\chi = 0.344$.

   c. The upper bound (equal energy criterion)—Equation 7 with $\chi = 1$.

   d. Compute risk of PTS for each of the three rules, assuming independence for two ears.

5. Repeat these steps for N_i = 300 simulated detonations.
6. For each dose-accumulation rule, average the risk computed at each point in the grid across the 300 simulations. Also determine the 97.5% and 2.5% risks for each grid point across the 300 simulations for each dose-accumulation rule. This forms a 95% confidence interval at each grid point.
7. Generate risk maps for different rules and input parameters.

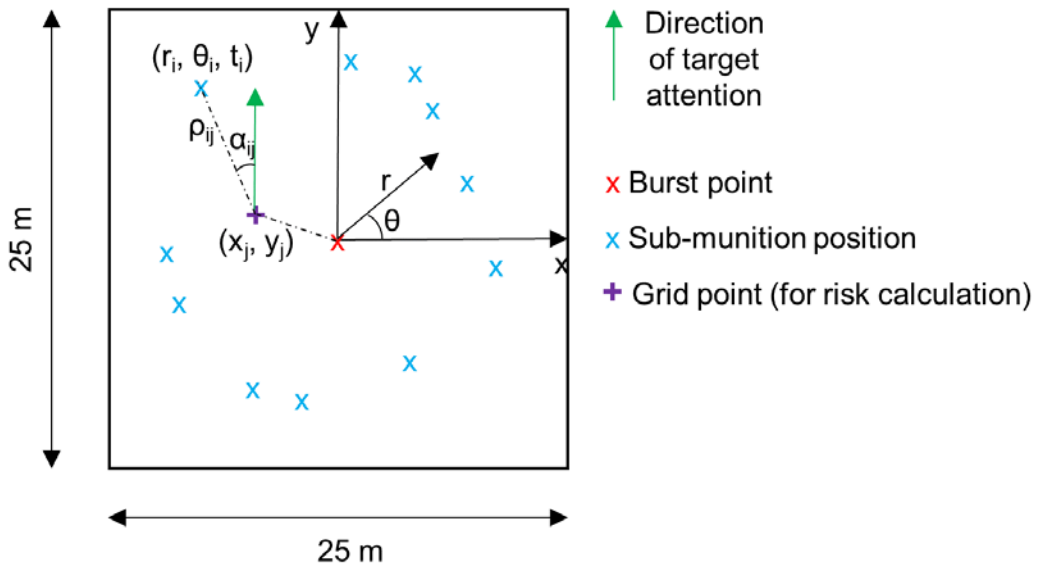

Figure 1. Diagram of Monte Carlo Simulation Approach. The diagram illustrates relevant quantities for calculating RSI for a single grid point (purple +), but calculations are done for an array of 625 grid points that fill the 25 × 25 m region.

Table 1 summarizes the sets of simulations conducted for this analysis and the varied parameter names, symbols, and values. Simulation 6 used the full set of default parameters. All other simulations except 24–27 used all but one of the default parameters (i.e., aside from simulation 6, each simulation varied only one parameter while keeping all other parameters at their default values). Simulations 24–27 varied K (the PTS threshold of interest, 25 dB; all other simulations used 40 dB), as well as either σ_f or $\bar{f}$, as shown in the table.

Table 1 also lists the set of values assumed by the varied parameter(s) for each set of simulations, with the default value shown in bold. Tables of mean risk in the 25 × 25 m scene, risk at the maximum risk radius, and maximum risk radial position can be found for all 27 simulations in Appendix B.

Table 1. Parameters Used in Monte Carlo Simulations

Simulation Set	Varied Parameter Name	Varied Parameter	Varied Parameter Values (default in bold)
1–7	Number of iterations	N_i	1, 10, 30, 50, 100, **300**, 1000
6, 8–9	Burst radius	R	**7**, 5, 10 m
6, 10–11	Burst radius standard deviation	σ_r	**1**, 0.5, 2 m
6, 12–16	Number of bursts	N_b	**11**, 1, 2, 5, 8, 14
6, 17–18	Average inter-pulse interval	$1/\lambda$	**150**, 100, 200 ms
6, 19–20	Pulse intensity standard deviation	σ_f	**2**, 1, 5 dB
6, 21–22	Pulse bias	$\bar{f}$	**0**, –5, 5 dB
6, 23	PTS threshold of interest	K	**40**, 25 dB
24, 25	Multiple parameters	K, σ_f	K = 25 dB, σ_f = 1, 5 dB
26, 27	Multiple parameters	K, $\bar{f}$	K = 25 dB, $\bar{f}$ = –5, 5 dB

This report often discusses risk as a function of radial position in the simulation, which also corresponds to distance from the mortar burst point. Therefore, both risk at the maximum risk radial position (unitless) and the maximum risk radial position itself were chosen as test variables for selecting an appropriate number of Monte Carlo iterations. In this report, we will refer to risk at the maximum risk radial position as "peak risk." Figure 2 shows the peak risk relative to the burst point as a function of the number of iterations. This value converged within 0.002 of the N_i = 1000 value within 50 iterations for all 3 methods of computing accumulated dose, and it is within 0.001 of the N_i = 1000 value for N_i = 300 for all 3 methods. This level of convergence is sufficient for analysis of effects in this report, which reports risks of injury to three decimal places (0.001).

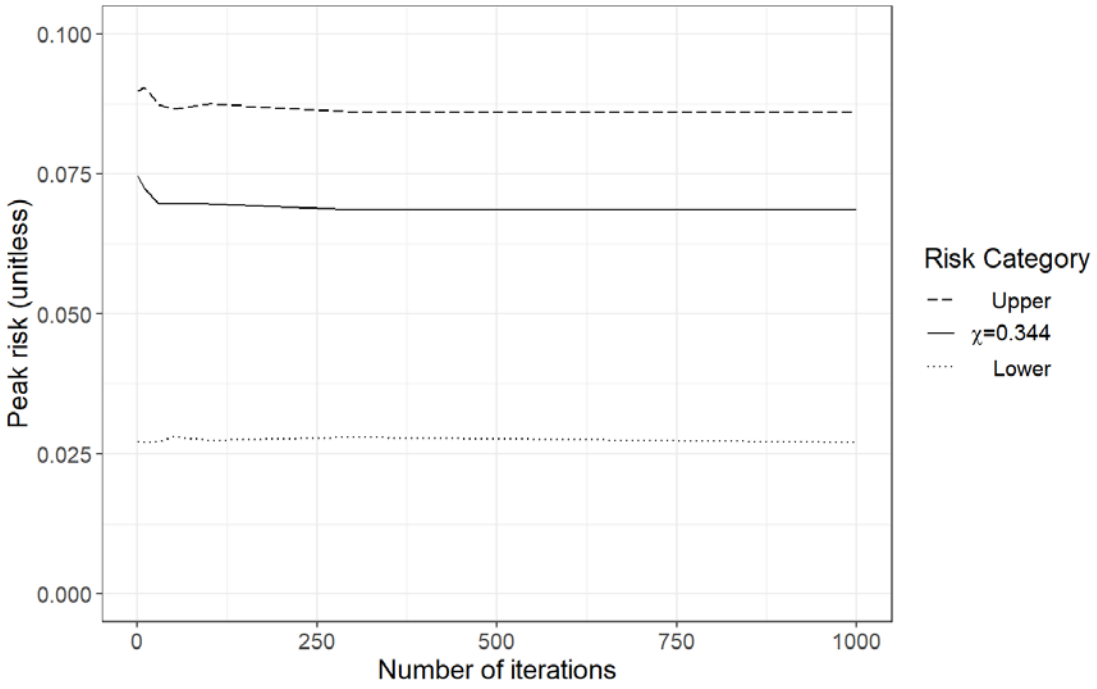

Figure 2. Peak Risk (risk of injury at the maximum risk radial position) as a Function of the Number of Iterations N_i in the Monte Carlo Simulation. Parameters for simulations: R = 7 m, σ_r = 1 m, N_b = 11, $1/\lambda$ = 150 ms, σ_f = 2 dB, $\bar{f}$ = 0 dB, K = 40 dB.

Figure 3 plots the radial position of maximum risk (relative to the burst point) as a function of the number of iterations N_i. At N_i = 300, the maximum risk radial position is within 0.2 m of the N_i = 1000 value for all three accumulated dose-computation methods. Since the simulation uses a 1 m square grid spacing, the radial resolution of the simulations is only about 0.22 m. Therefore, this level of convergence is representative of the accuracy that can be expected of the simulation.

These convergence tests show that 300 iterations provide sufficient precision (<0.001) for computing risk and sufficient spatial resolution (<0.2 m) to conduct analysis of the effects of the various parameter sets shown in Table 1 or the choice of dose-accumulation rule on risk maps. All simulations except for those in the convergence test series (1–7) were run with 300 iterations (N_i = 300).

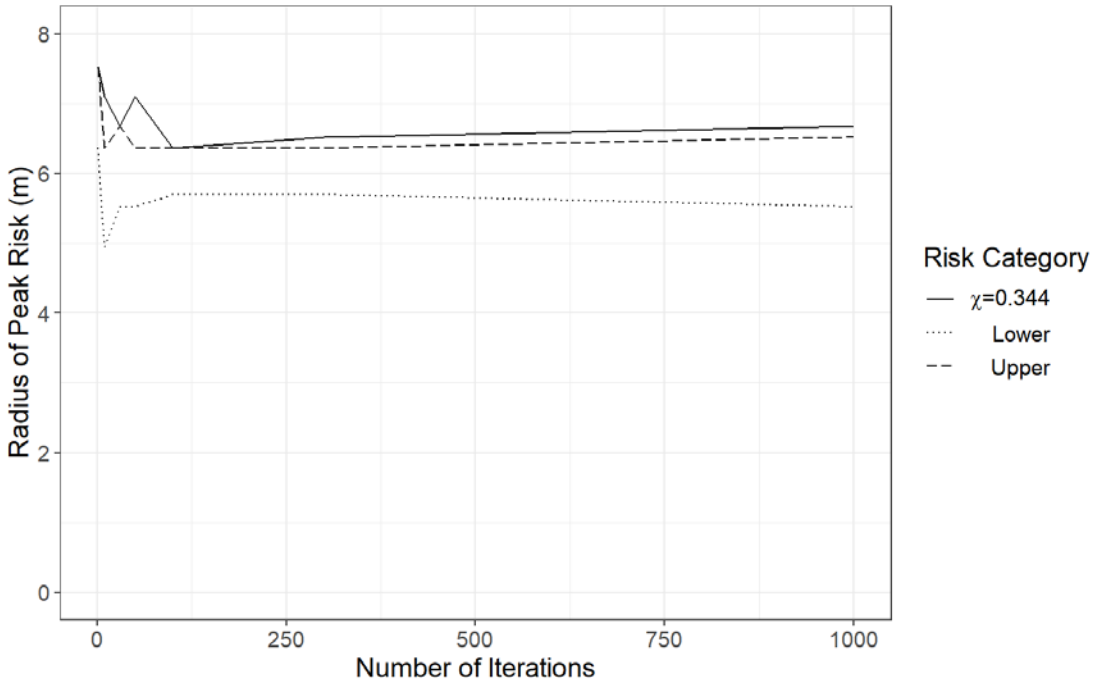

Figure 3. Maximum Risk Radial Position in Meters as a Function of the Number of Iterations N_i in the Monte Carlo Simulation. Note that "Upper" and "Lower" indicate the upper and lower bounds used to calculate *risk* (Figure 2), not the bounds on radial position of peak risk. Therefore, there is no requirement in this figure that the χ = 0.344 values be below the upper values and above the lower values. Parameters: R = 7 m, σ_r = 1 m, N_b = 11, $1/\lambda$ = 150 ms, σ_f = 2 dB, $\bar{f}$ = 0 dB, K = 40 dB.

3. Results and Discussion

Here, we present the results of the 27 Monte Carlo simulations. We begin with a discussion of the characteristics of risk maps generated by our simulations, which show risk as a function of position within the scene. Following this, a series of subsections discuss one or more varied parameters as described in Table 1, which appears in Section 2. We also include discussion of the uncertainties identified through our simulations and their relationships to certain variables of interest.

A. Risk as a Function of Position

Figure 4 shows RSI heat maps for the three methods of computing accumulated dose. The single-iteration heat maps on the left are representative of the risk profiles of an individual mortar burst. The spotty risk profile is indicative of the randomness with which submunitions land within the 25 × 25 m simulation zone. Some submunitions may be close together, producing areas of especially high risk, while other portions of the scene are far from any submunition, and exhibit low risk. For the $\chi = 0.344$ and $\chi = 1$ dose-accumulation rules (the reasonable estimate and upper bound methods), all submunitions contribute to risk, and so a large portion of the scene includes a risk of injury. But for the lower bound dose-accumulation rule, only the first submunition to detonate is counted (following Equation 10).[6] This means that the highest risk area of the simulation surrounds the position of the first submunition to detonate, rather than the positions of all submunitions, which is the case for the other two dose-accumulation methods.

With more iterations, risk is averaged for each position in the scene, and an annulus shape emerges because the simulation uses a uniform distribution for θ that becomes clear with many simulated detonations. Although it is difficult to see in the heat maps, the annulus shape is slightly off-center in the vertical direction because of the assumed $+y$ orientation of all subjects in these simulations. This orientation also means that positions at a $-y$ displacement relative to a given impulse will experience a slightly increased risk relative to those positioned at the same $+y$ displacement, due to angle-of-incidence effects.

[6] Note that the first submunition incorporates all impulse sounds that arrive at a given grid point within the first 50 ms of the pulse train, because these impulses will be combined following the procedure described in Section 2.

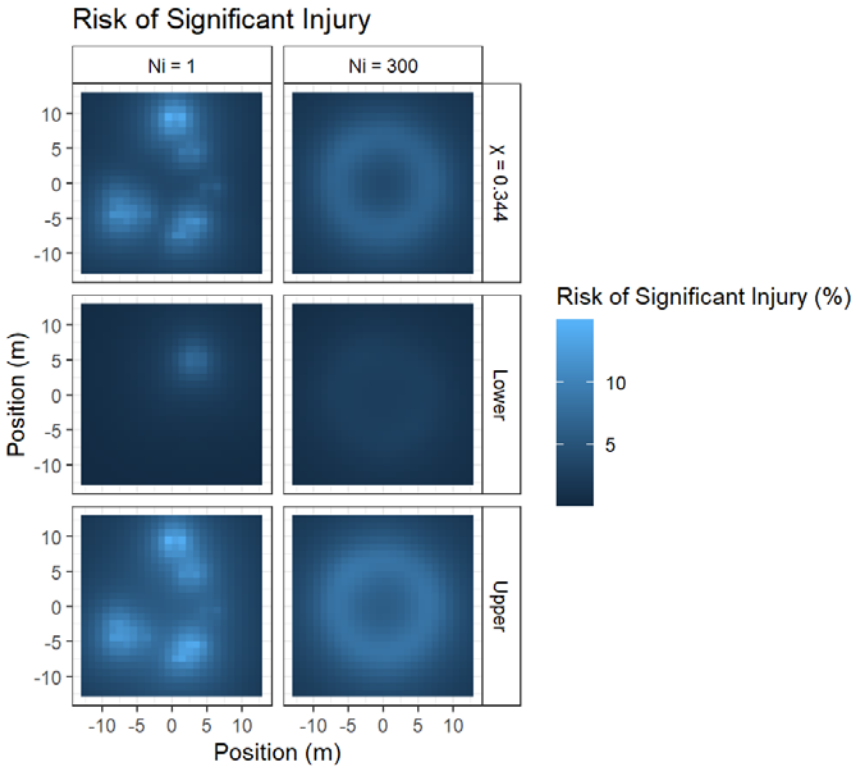

Figure 4. Heat Maps of Risk of PTS ≥ 40 dB as a Function of Position Averaged over N_i = 1 (left) or 300 (right) Simulations, and Using the Three Methods of Computing Dose Accumulation (top = χ = 0.344, middle = lower bound, bottom = upper bound). Averages are taken at each position over all N_i Monte Carlo simulations in a given run. Parameters for these plots: R = 7 m, σ_r = 1 m, N_b = 11, $1/\lambda$ = 150 ms, σ_f = 2 dB, $\bar{f}$ = 0 dB, K = 40 dB.

The heat maps show that the intensity of risk is greatest for the upper bound method of computing risk and least for the lower bound method, as expected. For the default parameter set, the average risk within the 25 × 25 m grid is 4.3% (1.8, 5.6), where we have reported values in the following format: estimate in percentage using χ = 0.344 dose-accumulation rule (lower bound estimate, upper bound estimate). This forms a bounded estimate of the expected risk for this set of parameters in the scene, depending on how dose accumulates. The expectation value for risk in the scene could be as high as 5.6% or as low as 1.8%, depending on the "true" dose-accumulation rule, or value of χ. Note that expected value for risk in the scene averages across all positions in the scene, effectively assuming a uniform density of subjects. If the scene contained a high density of subjects in some areas but not others, this would affect the aggregate RSI. It is also important to note that the average risk in the scene is affected by the scene size we chose to simulate. Larger scenes would produce lower scene-averaged risk because they include more area that is far from the site of the burst.

The data shown in the 300-iteration risk maps can be plotted as a function of radius for easier visual comparison of risks computed for simulations with different parameters.

Such plots, which take advantage of the cylindrical symmetry observed for the 300-iteration risk maps, average risk for points of equivalent radius in the scene. Further exploration of the nuances of these risk plots is available in Appendix A. We will use the term "peak risk" in this report to describe the maximum value in these risk vs. radius plots. Note, however, that individual Monte Carlo iterations will produce submunition patterns in which certain positions in the scene have higher risk than these peak values. This can be seen visually in Figure 4. The 300-iteration risk maps reflect *statistical expectation* as opposed to individual-iteration risk outcomes determined based on a known pattern of submunitions. The uncertainties in risk resulting from the pattern of submunitions are discussed further in Sections 3.B.2 and 3.D.

B. Burst Radius

We conducted a set of simulations varying the burst radius R from 5 to 10 m. This variation affects where submunitions land in the scene, as shown in Figure 5 for single iterations of each condition. Larger burst radii spread submunitions throughout the simulated area, while the smallest burst radius concentrates them in a tight area near the scene center.

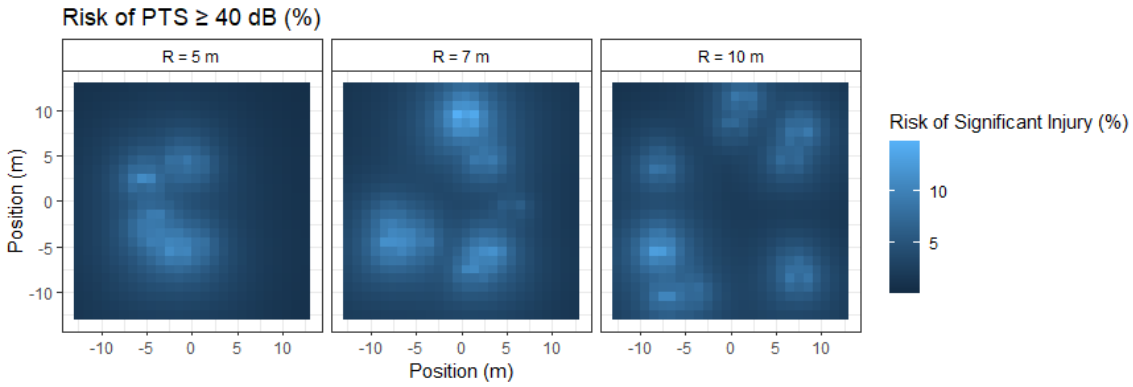

Figure 5. Heat Maps of Risk of PTS ≥ 40 dB as a Function of Position for N_i = 1 Simulation Using the χ = 0.344 Dose-Accumulation Rule for Burst Radii of 5 m (left), 7 m (center), and 10 m (right). Parameters for these plots: N_i = 1, σ_r = 1 m, N_b = 11, $1/\lambda$ = 150 ms, σ_f = 2 dB, $\bar{f}$ = 0 dB, K = 40 dB.

Figure 6 plots the risk of PTS ≥ 40 dB as a function of radius (distance from the burst point) for three different burst radii R, as determined based on the 300-iteration averaged results. Table 2 lists the peak risk and mean risk averaged over the 25 × 25 m scene for simulations with R varied from 5 to 10 m.

In general, risk peaks at a radius that is slightly less than R because subjects inside the risk annulus are on average closer to the set of submunitions than subjects outside the

annulus by the same distance, so the subjects in the interior receive larger (and therefore riskier) doses.

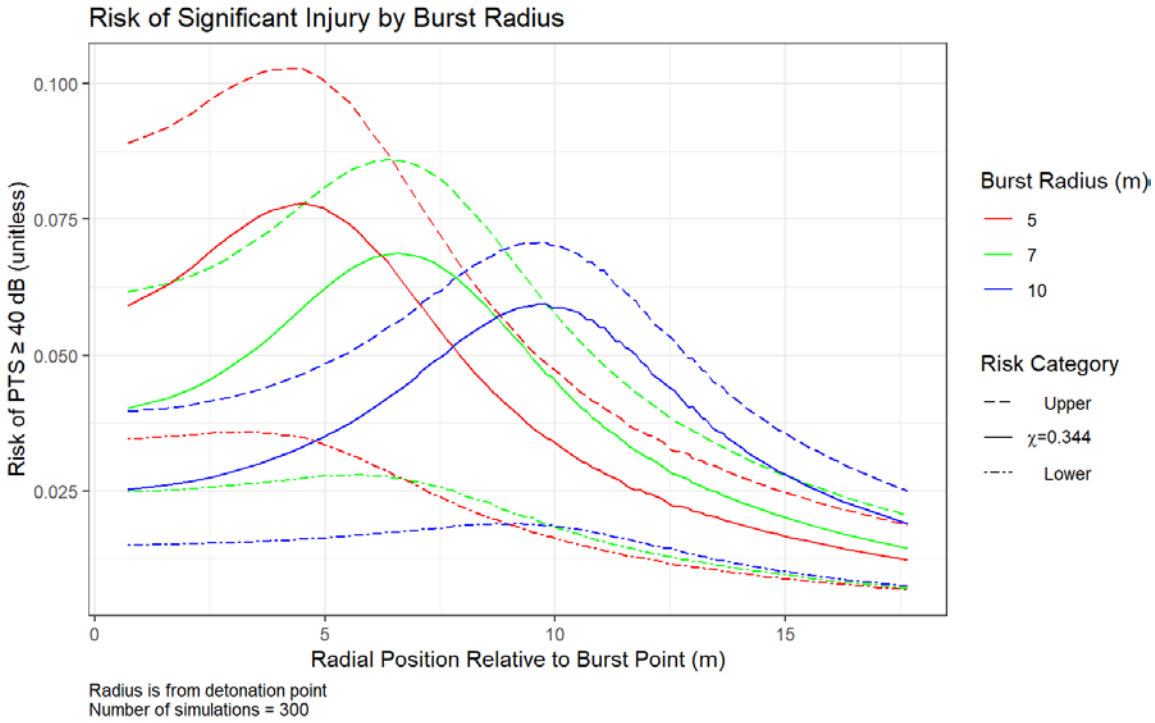

Figure 6. Risk of PTS ≥ 40 dB as a Function of Radial Position Relative to the Burst Point within the 25 × 25 m Simulation Grid for Three Values of Burst Radius *R*. Red lines indicate *R* = 5 m, green lines indicate *R* = 7 m, and blue lines indicate *R* = 10 m. Solid lines estimate risk using the χ = 0.344 dose-accumulation rule. Dashed lines use the upper bound dose-accumulation rule with χ = 1. Dash-dotted lines use the lower bound dose-accumulation rule defined in Equation 10. Parameters for these simulations: N_i = 300, σ_r = 1 m, N_b = 11, $1/\lambda$ = 150 ms, σ_f = 2 dB, $\bar{f}$ = 0 dB, K = 40 dB.

Table 2. Peak Risk and Scene-Averaged Risk for Differing Burst Radius *R*

Burst Radius *R* (m)	Peak Risk			Scene-Averaged Risk		
	Risk (%) (Equation 10)	Risk (%) for χ = 0.344	Risk (%) for χ = 1	Risk (%) (Equation 10)	Risk (%) for χ = 0.344	Risk (%) for χ = 1
5	3.6	7.8	10.3	1.8	3.9	5.4
7	2.8	6.9	8.6	1.8	4.3	5.6
10	1.9	5.9	7.1	1.6	4.4	5.5

Parameters for these simulations: N_i = 300, σ_r = 1 m, N_b = 11, $1/\lambda$ = 150 ms, σ_f = 2 dB, $\bar{f}$ = 0 dB, K = 40 dB.

As shown in Figure 6, with increasing burst radius *R*, the peak risk decreases, while the position of the peak moves outward, tracking the burst radius. Thus, *larger burst radii* (*distributing submunitions over a wider area*) *reduce the expected peak risk while*

spreading risk more evenly within the 25 × 25 m zone. These effects occur for all three dose-accumulation rules. Note again that *peak risk* refers to the maximum of the statistical expectation value of RSI as a function of radius (based on 300 iterations of the simulation). This is distinct from the maximum risk at any point in a scene for a single iteration, which may be higher than this peak, as shown in Figure 5, where certain positions end up with risks exceeding 11%.

The change in burst radius also causes the risk averaged across the 25 × 25 m exposure region to increase for the $\chi = 0.344$ and $\chi = 1$ rules, as impulses cover the region more evenly. This effect does not occur for the lower bound rule, which only accounts for the first impulse in computing dose. Note that larger scenes with the same submunition-distributing mortar device would have lower values of scene-averaged risk. Also note that trends in average risk may be affected by the size of the simulated zone (as well as distribution of subjects, if a non-uniform subject distribution is assumed) because larger simulations include more space that is far from the actual device. In general, RSI computations should be focused on the target area where human effects are expected, since scene-averaged RSI values will tend to obscure information about the presence and size of high-risk zones.

In the subsections that follow, we will discuss how the position of a target within the scene relates to different uncertainties in risk estimation.

1. Dose-Accumulation Uncertainty

Analyzing these charts in more detail, we see that the relative importance of the dose-accumulation-rule uncertainty increases in the low-risk regime. Using as an example the $R = 5$ data shown in red in Figure 6, the peak risk (at a position of ~4.5 m) is 7.8% (3.6, 10.3) based on the three different methods of computing dose accumulation, at an uncertainty Δ_d of 6.7 percentage points. At a radial position of 15 m, the injury risk is estimated at 1.7% (0.9, 2.5), at an uncertainty Δ_d of only 1.6 percentage points. Δ_d is 86% of the value of risk at the 4.5 m position (7.8) and 94% of the value of risk at the 1.7 m position (1.7),[7] indicating that the uncertainty related to the dose-accumulation rule is more important, in a relative sense, in the low-risk zone. One explanation may be that in the high-risk zone of this simulation (near a radial position of 4.5 m), targets are likely to have at least one impulse at close range, providing a large contribution to risk relative to the other impulses. This is visually clear in the example shown in Figure 5, where more than 50% of the circumference of the annulus at a radius of 4.5 m is covered by a bright spot from a submunition. In contrast, in the low-risk zone of the simulation, all impulses are individually fairly low risk, meaning that the method of aggregation plays an important role in determining risk for the full exposure. Table 3 summarizes the risk ranges derived

[7] 6.7/7.8 = 0.86, 1.6/1.7 = 0.94

from the dose-accumulation rule, as well as some other uncertainties that are discussed in the next sections.

Table 3. Risk and Associated Uncertainties Derived from Various Sources for Simulation with R = 5 m

Radial Position (m)	Risk (%) for χ = 0.344	Dose Accumulation Rule Δ_d (3.B.1)	Submunition Pattern CI_p (3.B.2)	Auditory 4.5 CI_a (3.B.3)
4.5	7.8	6.7	7.5	6.9
15	1.7	1.6	1.2	1.8

Uncertainties are reported as percentages. Δ_d is defined as the difference between the *expected* risk values computed for the χ = 1 and Equation 10 dose-accumulation rules. CI_p is the 95% confidence interval for risk at the specified radial position with the χ = 0.344 dose-accumulation rule determined through Monte Carlo simulation of many submunition patterns. CI_a is defined as the 95% confidence interval for two-eared risk determined based on the injury risk at the specified radial position for the χ = 0.344 dose-accumulation rule and under the assumption that both ears have the same risk (effectively, grazing incidence exposure). Values are pulled from simulation with parameters: N_i = 300, R = 5 m, σ_r = 1 m, N_b = 11, $1/\lambda$ = 150 ms, σ_f = 2 dB, $\bar{f}$ = 0 dB, K = 40 dB.

2. Uncertainty Due to the Pattern of Submunitions

Figure 7 breaks the data shown in Figure 6 into nine panels that display confidence intervals of risk as a function of radial position for each combination of dose-accumulation rule and burst radius R. These 95% confidence intervals CI_p are not bounds on *expected* risk (a statistical expectation value that is based on an average of many simulations), but rather an indication of the possible *range* of risk vs. radial position values that may occur for individual iterations of the Monte Carlo simulation and a fixed dose-accumulation rule. In other words, these confidence intervals describe the range of possible risk that a person at a given radial position in the scene could experience in a single multi-impulse exposure, based on a fixed dose-accumulation rule. CI_p primarily reflects uncertainty related to the pattern of submunitions.

Reviewing the data shown in Table 3 and Figure 7, we see the 95% confidence interval for risk computed across 300 simulated bursts with the χ = 0.344 rule and a burst radius of 5 m is (4.1, 11.6), or a range of 7.5 percentage points, at a radial position of 4.5 m. At a radial position of 15 m, this interval is (1.2, 2.4), or a range of 1.2 percentage points. These values translate to 96% and 71% of the expected risk values computed at their respective radial positions using the χ = 0.344 rule.

These results illustrate how the sensitivity of risk to the pattern of submunitions depends on the relative proximity to the maximum risk region. The risk to individuals standing in the most hazardous zone will be quite sensitive to the pattern of submunitions, while the risk to those standing farther from that zone will be less sensitive to the pattern of submunitions.

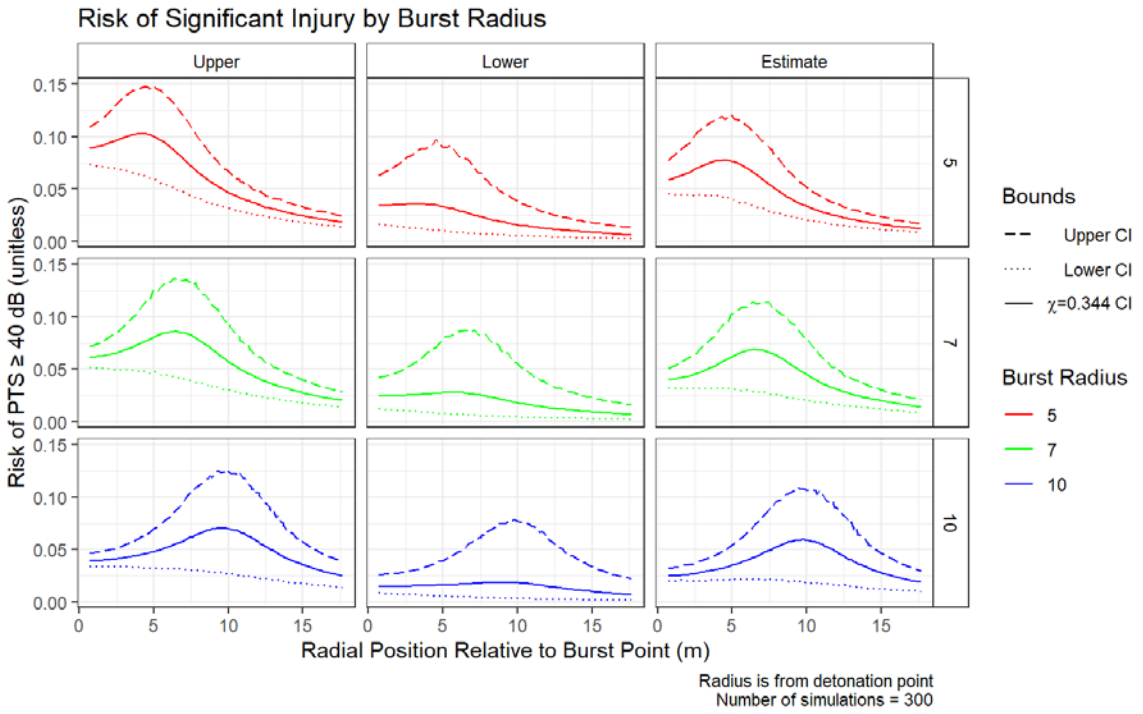

Figure 7. Risk of PTS ≥ 40 dB as a Function of Radial Position Relative to the Burst Point within the 25 × 25 m Simulation Grid for Three Values of Burst Radius *R*. Each plot shows the expected RSI value as a function of radius, as well as the 95% confidence interval (CI) for that radial position based on Monte Carlo simulation results. Red lines (top row) indicate *R* = 5 m, green lines (center row) indicate *R* = 7 m, and blue lines (bottom row) indicate *R* = 10 m. The left column uses the upper bound dose-accumulation rule with *χ* = 1. The center column uses the lower bound dose-accumulation rule defined in Equation 10. The right column uses the *χ* = 0.344 dose-accumulation rule. Parameters for these plots: N_i = 300, σ_r = 1 m, N_b = 11, $1/\lambda$ = 150 ms, σ_f = 2 dB, $\bar{f}$ = 0 dB, *K* = 40 dB.

3. Auditory 4.5 Uncertainty

A third type of uncertainty range CI_a can be identified based on the Auditory 4.5 model itself. At the 4.5 m radial position, the two-eared RSI of 7.8% computed with the χ = 0.344 rule corresponds to a single-ear RSI of about 4% (based on two ears with equal risk and the assumption of independence Equation 12). At this level of risk, the confidence interval computed by Auditory 4.5 is (5.3, 3.4), where we have accounted for both the model-fitting error (computed using Auditory 4.5's built-in confidence intervals) and the uncertainty in the human-to-chinchilla parameter *C* determined in previous work (Swallow and Kramer 2019), as described in Appendix B. At 15 m, the single-ear risk is 0.9%, and the confidence interval for that risk is (0.5, 1.4). Extending these single-ear confidence intervals to the two-eared case (following Equation 12), we obtain confidence intervals for the two-eared risk regime of (3.4, 10.3) at 4.5 m and (1, 2.8) at 15 m, corresponding to ranges CI_a of 6.9 and 1.8 percentage points, respectively. With reference to Table 3, these intervals correspond to 88% and 105% of the expected risk computed with the χ = 0.344 rule at their respective radial positions.

These results demonstrate an example where the uncertainty due to the dose-accumulation rule for multi-impulse, short-IPI exposures is of similar magnitude to the uncertainty of risk estimates based on the Auditory 4.5 model. The magnitude of CI_a is a function of the input value A and only depends on the number of impulses to the extent that this changes A. This uncertainty range derives from the source data used to develop Auditory 4.5, which used exposures with multiple impulses of equivalent intensity and IPI > 1 s. Some component of uncertainty in dose accumulation is contained within Auditory 4.5's model-fitting error; however, it is not possible to state what proportion of the uncertainty is solely due to this source, as opposed to other factors (e.g., subject biovariability, accuracy of sound output recordings, etc.). We shall see that for the risk-bounding-analysis approach (which applies to the case of multi-impulse exposures with IPI < 1 s), the uncertainty due to the dose accumulation increases strongly with increasing N_b, the number of impulses (see Section 3.D), while the uncertainty contained in the Auditory 4.5 model is of consistent relative size to the overall risk estimated. Therefore, the need to account for dose-accumulation uncertainty becomes more important as the number of impulses increases.

4. Burst Radius Uncertainty

Figure 8 displays the effect of the uncertainty in the burst radius σ_r on the overall risk vs. radial position profile. Table 4 lists the peak risk and mean risk averaged over the 25 × 25 m scene for simulations with σ_r varied from 0.5 to 2 m.

For the $\chi = 1$ and $\chi = 0.344$ dose-accumulation rules, increased uncertainty in burst radius causes a slight decrease in the maximum risk radial position and a slight depression in the peak risk, broadening risk more across the exposed area. This has the side effect of also very slightly increasing the average risk in the 25 m × 25 m scene. For individual iterations, there will still be positions with very high risk regardless of σ_r. However, increased σ_r causes individual submunitions to be dispersed over an annular area, which spreads out their associated risk and lowers the peak risk slightly because they are less concentrated at a specific radius. The $\chi = 1$ and $\chi = 0.344$ dose-accumulation rules compound the effects of uncertainty in overall dose accumulation that are ignored by the lower bound rule; this is why the effect for the lower bound is fairly insignificant. These effects are also smaller than those observed for changes in the actual burst radius R, but are nonetheless important in that they convey how *greater precision in device dispersion in the scene* (*decreased* σ_r) *also contributes to decreased uniformity in overall risk, increased peak risk in a scene, and decreased average risk in the scene.*

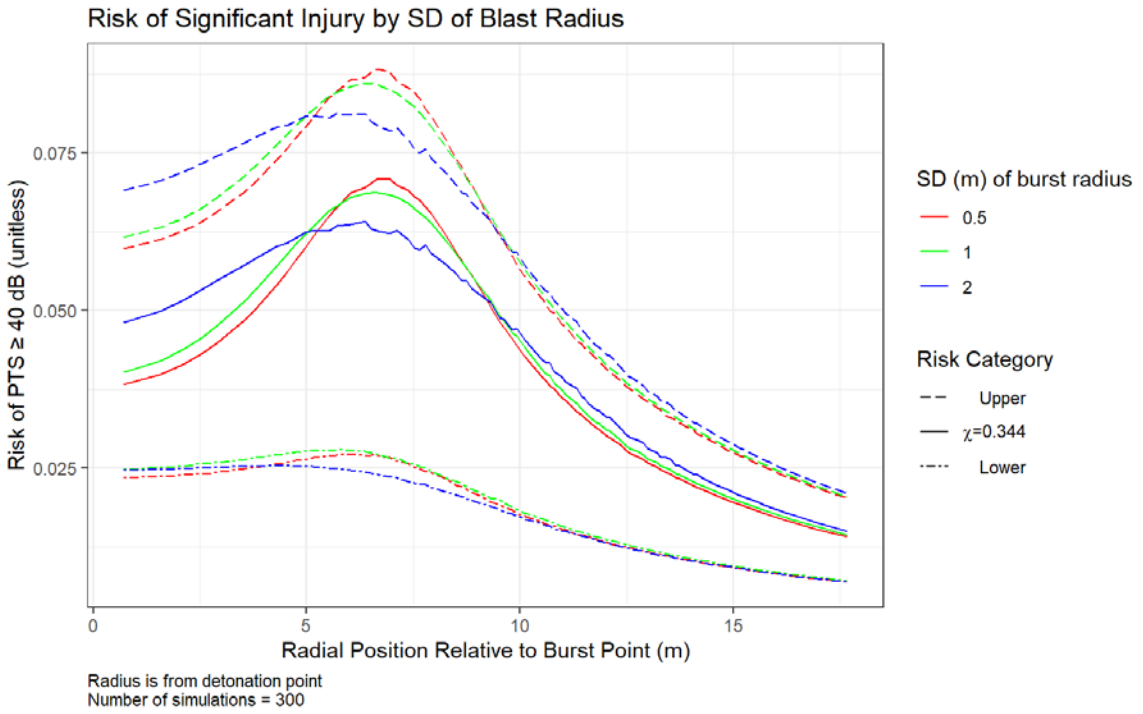

Figure 8. Risk of PTS ≥ 40 dB as a Function of Radial Position Relative to the Burst Point within the 25 × 25 m Simulation Grid for Three Values of Burst Radius Standard Deviation σ_r. Red lines indicate σ_r = 0.5 m, green lines indicate σ_r = 1 m, and blue lines indicate σ_r = 2 m. Solid lines estimate risk using the χ = 0.344 dose-accumulation rule. Dashed lines use the upper bound dose-accumulation rule with χ = 1. Dash-dotted lines use the lower bound dose-accumulation rule defined in Equation 10. Parameters for these plots: N_i = 300, R = 7 m, N_b = 11, $1/\lambda$ = 150 ms, σ_f = 2 dB, $\bar{f}$ = 0 dB, K = 40 dB.

Table 4. Peak Risk and Scene-Averaged Risk for Differing Burst Radius Standard Deviation σ_r

Burst Radius Standard Deviation σ_r (m)	Peak Risk			Scene-Averaged Risk		
	Risk (%) (Equation 10)	Risk (%) for χ = 0.344	Risk (%) for χ = 1	Risk (%) (Equation 10)	Risk (%) for χ = 0.344	Risk (%) for χ = 1
0.5	2.7	7.1	8.8	1.8	4.2	5.5
1	2.8	6.9	8.6	1.8	4.3	5.6
2	2.5	6.4	8.1	1.7	4.3	5.6

Parameters for these simulations: N_i = 300, R = 7 m, N_b = 11, $1/\lambda$ = 150 ms, σ_f = 2 dB, $\bar{f}$ = 0 dB, K = 40 dB.

5. Management of Uncertainty

Note that the uncertainties described here can be managed in various ways. The number of impulses and the uncertainty in the distribution radius of submunitions are both design parameters that can be adjusted, depending on the uncertainty the designer is willing to tolerate. These will have an impact on the uncertainty of the risk maps for the device.

But the uncertainty due to dose accumulation for a fixed number of impulses within the acoustic-reflex regime (inter-pulse intervals below 1 s) will only be possible to narrow through the collection of experimental data (likely from animal subjects) or analysis of past multi-impulse exposures of humans, ideally in conjunction with biofidelic modeling. Much of the uncertainty contained within Auditory 4.5's confidence intervals results from natural variation in the subjects used to build the model and therefore is unlikely to be substantially reduced through additional experimental data collected outside the acoustic reflex regime, because the data used to build the model were already extensive.

C. Inter-pulse Interval

The effect of the IPI parameter $1/\lambda$ in the simulations is subtle. In the simulation, $1/\lambda$ is the average spacing in time between submunition detonations. If two submunitions detonate in close temporal proximity defined by the threshold of 50 ms, the energy from those two bursts is summed using the equal-energy criterion ($\chi = 1$ rule), following the logic that this time period (50 ms) is too short for the acoustic reflex to engage or for the ear to distinguish these impulses. The result is that the intensity of one of the bursts increases while the total number of bursts decreases by one. The overall dose by the $\chi = 0.344$ rule should be increased by these combined-burst events when they happen. For the lower bound (Eq. 8) dose-accumulation rule, the total dose is only affected if the combined-burst event is the first impulse heard by the target. In such cases, however, the total dose is increased by several decibels. The frequency of these combined-burst events is greatest for smaller values of $1/\lambda$, which should translate to a small increase in the total injury risk observed. However, once $1/\lambda$ is large enough that these combined-burst events rarely happen, further increases in $1/\lambda$ have no effect on the injury risk profiles.

Figure 9 shows that the effect of varying $1/\lambda$ is small relative to the uncertainty in RSI caused by uncertainty in the dose-accumulation rule itself. A modest decrease in risk is observed for the longest IPI, but the effect is only a few tenths of a percentage point at its largest.

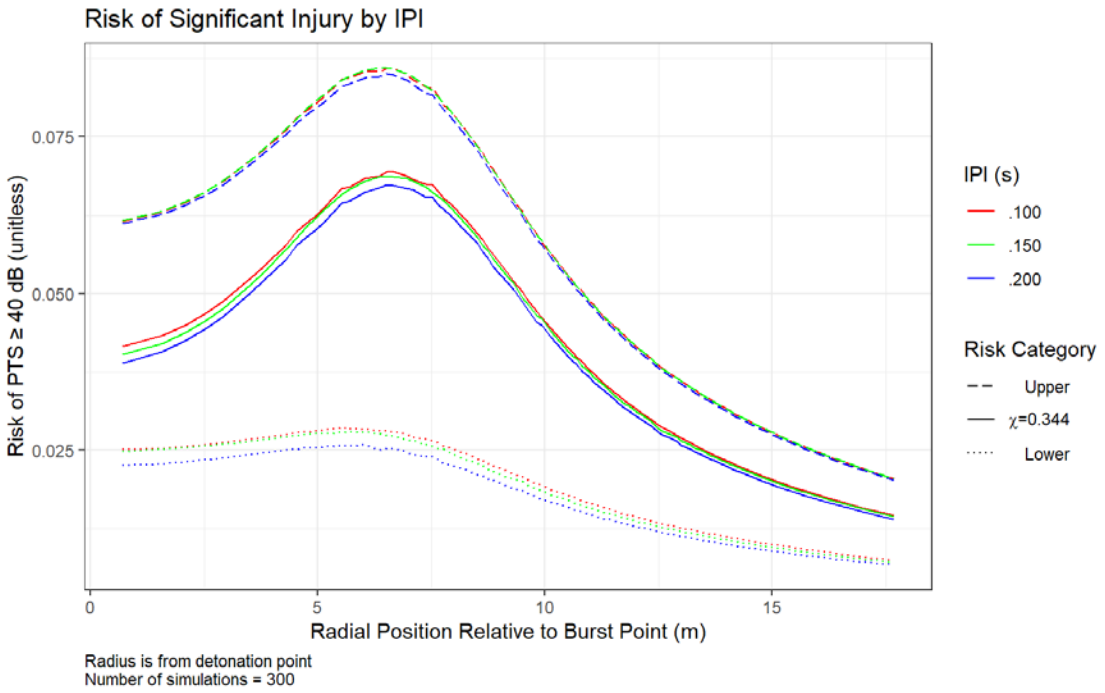

Figure 9. Risk of PTS ≥ 40 dB as a Function of Radial Position Relative to the Burst Point within the 25 × 25 m Simulation Grid for Three Values of IPI *1/λ*. Red lines indicate 1/*λ* = 100 ms, green lines indicate 1/*λ* = 150 ms, and blue lines indicate 1/*λ* = 200 ms. Solid lines estimate risk using the *χ* = 0.344 dose-accumulation rule. Dashed lines use the upper bound dose-accumulation rule with *χ* = 1. Dotted lines use the lower bound dose-accumulation rule defined in Equation 10. Parameters for these plots: N_i = 300, R = 7, σ_r = 1 m, N_b = 11, σ_f = 2 dB, $\bar{f}$ = 0 dB, K = 40 dB.

D. Number of Impulses

Next, we explore the effect of the number of impulses. This design parameter is relevant not only for weapons designed with multiple submunitions in one mortar, but also for circumstances in which multiple flashbang devices are used in an area in rapid succession. Although our simulation is a better representation of the mortar case, some of our findings also apply to the second case.

Figure 10 plots risk vs. radial position relative to the burst for the different values of N_b and the three dose-accumulation rules. These charts show how the risk grows with the number of submunitions for the rules with nonzero χ. In contrast, the lower bound risk estimate remains largely unaffected as N_b grows.[8] The effect of N_b is largest in the high-risk (peaked) region of the curve—increased numbers of submunitions have little effect on

[8] In fact, there is a modest increase in lower bound risk moving from N_b = 1 to N_b = 2, which is attributed to two factors: first, in multi-impulse exposures, the first impulses occasionally occur close enough together in time (<50 ms apart) to be treated as a single impulse of greater intensity, and second, under special circumstances, an impulse that detonates later in time is heard earlier than a prior impulse because of proximity and the speed of sound travel. Both these factors will cause an increase in estimated risk when they occur.

RSI when a subject is standing at an already low-risk position. As a specific example, the risk at the 15 m radial position for N_b = 14 is less than the peak risk for N_b = 2. Another way to think about this is that for nonzero χ, the worst case radial position risk grows much faster than the wide-area risk when adding more submunitions. This also suggests that spreading out submunitions in an area could help reduce the intensity of "hot spots" in an individual multi-submunition exposure.

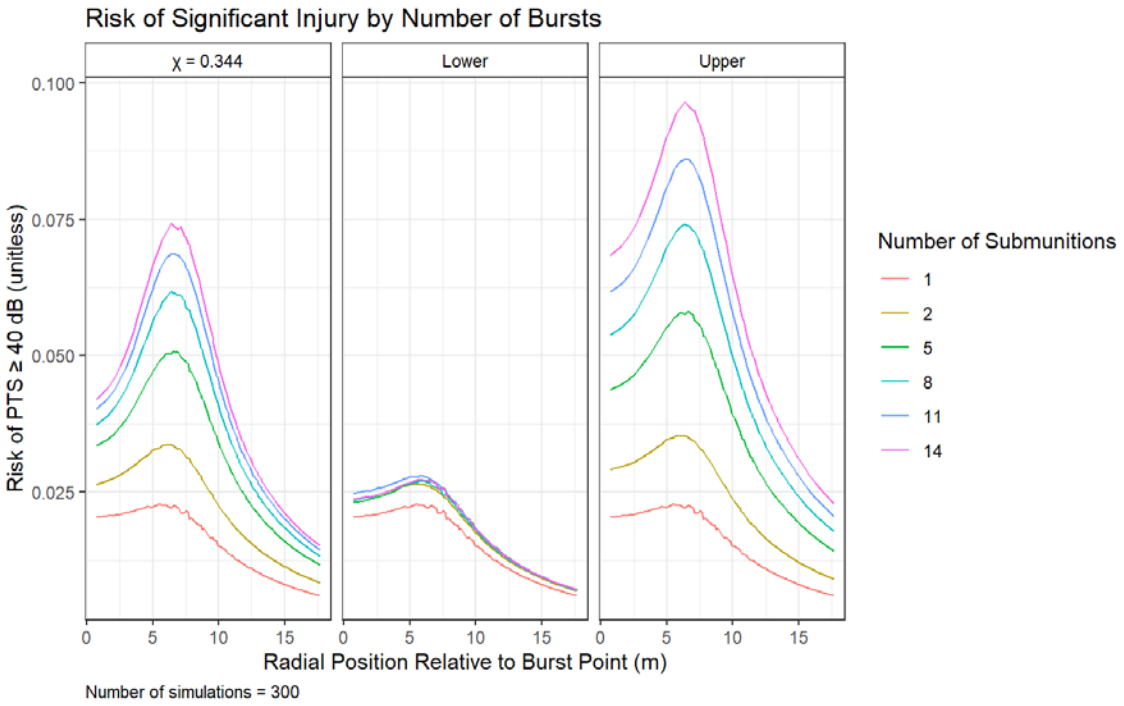

Figure 10. Risk of PTS ≥ 40 dB as a Function of Radial Position Relative to the Burst Point in the 25 × 25 m Scene. Line color indicates the number of submunitions N_b. Left column estimates risk using the χ = 0.344 dose-accumulation rule. Middle column uses the lower bound dose-accumulation rule defined by Equation 10. Right column uses the upper bound dose-accumulation rule with χ = 1. Parameters for these plots: N_i = 300, R = 7, σ_r = 1 m, $1/\lambda$ = 150 ms, σ_f = 2 dB, $\bar{f}$ = 0 dB, K = 40 dB.

This is seen more clearly by considering Figure 11, which shows that both the peak risk and the average risk in the scene increase as a function of the number of submunitions N_b for both χ = 0.344 and χ = 1 (upper bound) dose-accumulation rules. The slopes of risk as a function of N_b for the χ = 0.344 and χ = 1 rules are noticeably steeper for the maximum risk than for the scene-averaged risk. For the lower bound (Equation 10) rule, additional submunitions do not increase RSI after N_b = 2 because for this rule, only the first submunition is counted.[9] Increasing the number of submunitions does not affect the likelihood that the first submunition lands close to any particular location in the scene, so

[9] Ibid.

positional variation caused by this effect average out over the 300 iterations, as shown in Figure 4.

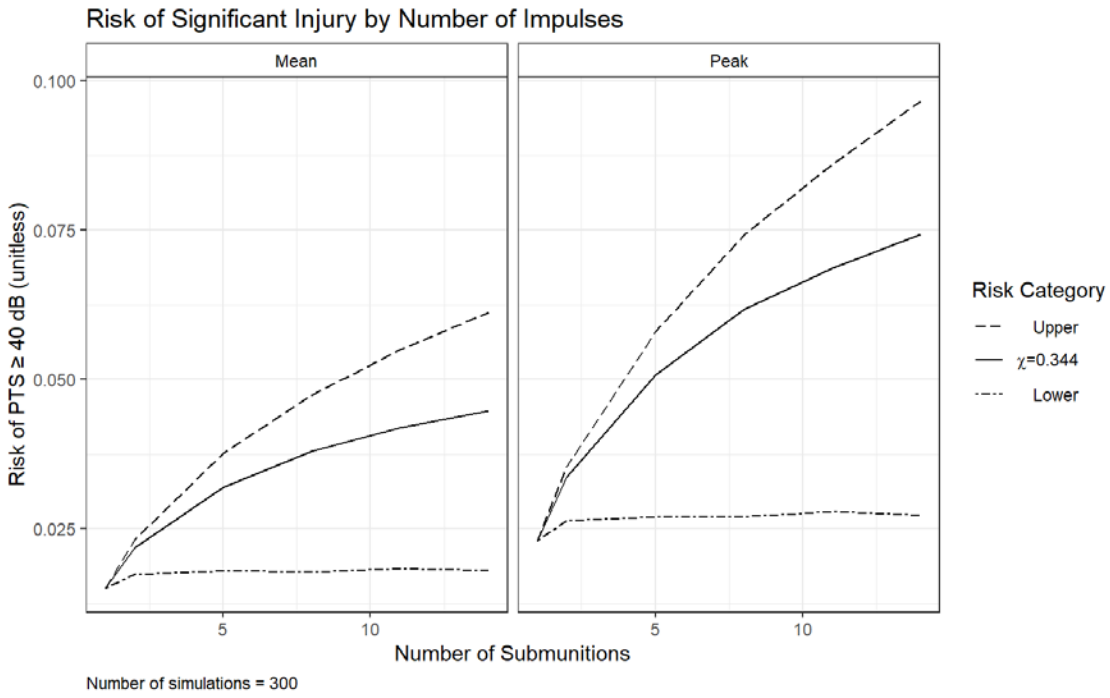

Figure 11. Risk of PTS ≥ 40 dB (left) Averaged across the 25 × 25 m Scene and (right) Computed at the Maximum Risk Radius in the 25 × 25 m Scene (peak risk) as a Function of Number of Bursts N_b for Three Dose-Accumulation Rules. Solid lines estimate risk using the $\chi = 0.344$ dose-accumulation rule. Dashed lines use the upper bound dose-accumulation rule with $\chi = 1$. Dash-dotted lines use the lower bound dose-accumulation rule defined in Equation 10. Parameters for these plots: $N_i = 300$, $R = 7$, $\sigma_r = 1$ m, $1/\lambda = 150$ ms, $\sigma_f = 2$ dB, $\bar{f} = 0$ dB, $K = 40$ dB.

The deviation between the risk estimated using the $\chi = 0.344$ rule and the lower bound grows faster than the deviation between the $\chi = 0.344$ rule and the upper bound, because the lower bound remains constant with N_b while the upper bound and $\chi = 0.344$ estimates grow. This result illustrates that *uncertainty about the role of the acoustic reflex in protecting targets from significant injury becomes more important when multi-impulse tactics and devices are employed in short* (*second-scale*) *time intervals*. Because we do not fully understand the dose accumulation for flashbang-type impulses at short time scales, devices and training must be designed with deference to the high-risk end of the uncertainty spectrum ($\chi = 0.344$ to $\chi = 1$ rule), even though it is possible that short IPIs actually result in reduced risk, possibly without impeding device effectiveness. However, little data exist to validate this claim, including no data on the human effectiveness of multi-impulse flashbang designs relative to single-impulse designs. This lack of data impedes the ability to design devices that best balance RSI and effectiveness.

Note that setting χ to a very small value (e.g., 0.01) would have the effect of computing risk based on the impulse with *maximum* A_j relative to a given position in the scene, rather than based on the first impulse to occur. We should expect such a dose-accumulation rule to produce RSI estimates that fall between the $\chi = 0.344$ estimate and the Equation 10 lower bound. Under such a scheme, increasing the number of submunitions would increase the likelihood that *at least one* submunition falls near a given position, thus increasing expected risk throughout the scene. Although setting χ near 0 is not a lower bound on the possible protective effect of the acoustic reflex (which may be triggered before the loudest impulse occurs), it would be a reasonable alternative accumulation rule under an assumption such as *the acoustic reflex engages only for the loudest impulses*. An improved version, if data were available to support it, would mix the role of timing and intensity, such that risk was computed based on an assumption that the acoustic reflex engages after the first impulse that exceeds a certain intensity threshold. But obtaining the data to support such an approach would be challenging and likely require some extrapolation of effects from animal subjects to humans.

Finally, we consider how the number of submunitions affects the uncertainty ranges for risk derived from various sources. Table 5 provides a summary of the uncertainty ranges derived from three sources for the simulations with $N_b = 2$ and $N_b = 14$. These are the same three uncertainty ranges Δ_d, CI_p, and CI_a discussed in Section 3.B. In absolute terms, the uncertainty range CI_p hardly changes with increased N_b, while CI_a increases somewhat and Δ_d increases substantially.

Considered relative to the peak risk values for these conditions, the relative size[10] of Δ_d increases rapidly with increased N_b, the relative size of CI_a remains about the same (slight decrease), and the relative size of CI_p decreases. In other words, *adding more submunitions adds uncertainty to our estimates of expected peak risk due to our uncertainty in the dose-accumulation rule, while decreasing the relative uncertainty in estimated risk in a scene related to the pattern of submunitions*.

Table 5. Peak Risk and Associated Uncertainty Ranges Derived from Various Sources for Simulations with Varied N_b

N_b	Peak Risk (%) for χ = 0.344	Dose-Accumulation Rule Δ_d	Submunition Pattern CI_p	Auditory 4.5 CI_a
2	3.4	0.9	8.0	3.9
14	7.4	7.0	8.2	6.8

Peak risk ranges are reported as percentages. Δ_d is defined as the difference between the *expected* risk values computed for the $\chi = 1$ and Equation 10 dose-accumulation rules. CI_p is the 95% confidence interval for peak risk with the $\chi = 0.344$ dose-accumulation rule determined through Monte Carlo

[10] In the context of this discussion, "relative size" of an uncertainty range is defined as the ratio of the uncertainty range Δ_d, CI_p, or CI_a to the peak risk estimate using the $\chi = 0.344$ dose-accumulation rule. For example, with reference to Table 3, the relative size of Δ_d for $N_b = 2$ is 0.9/3.4 = 26%.

simulation of many submunition patterns. CI_a is defined as the 95% confidence interval for two-eared risk determined based on the peak risk for the $\chi = 0.344$ dose-accumulation rule and under the assumption that both ears have the same risk (effectively, grazing incidence exposure). Values are pulled from simulation with parameters: $N_i = 300$, $R = 7$ m, $\sigma_r = 1$ m, $N_b = 2$ or 14, $1/\lambda = 150$ ms, $\sigma_f = 2$ dB, $\bar{f} = 0$ dB, $K = 40$ dB.

Auditory 4.5 does include a built-in dose-accumulation rule that can be applied in specific circumstances (equal impulse intensity, IPI > 1 s), and some of the uncertainty related to that rule is built in to the model's overall confidence intervals. However, additional uncertainty emerges when we enter the acoustic reflex regime with individual impulses of unequal intensity spaced closely in time. Our analysis shows that this uncertainty can be substantial for large numbers of submunitions and should not be ignored.

Table 6 displays the scene-averaged risks and associated risk ranges Δ_d and CI_a computed for $N_b = 2$ and $N_b = 14$. CI_p could not be computed because the full scene-averaged risk was not stored for each iteration of the Monte Carlo. Table 6 shows that the trends observed for the peak risk are consistent for the scene-averaged risk for both Δ_d and CI_a; the relative size of Δ_d increases substantially (from 23% to 96%) with increased N_b, and the relative size of CI_a decreases. Therefore, the dose-accumulation-rule-derived uncertainty is important for understanding both peak and average risk in a scene with many impulses.

Table 6. Scene-Averaged Risk and Associated Uncertainty Ranges Derived from Various Sources for Simulations with Varied N_b

N_b	Scene-Averaged Risk (%) for $\chi = 0.344$	Dose-Accumulation Rule Δ_d	Auditory 4.5 CI_a
2	2.2	0.5	2.8
14	4.6	4.4	3.3

Scene-averaged risk ranges are reported as percentages. Δ_d is defined as the difference between the *expected* risk values computed for the $\chi = 1$ and Equation 10 dose-accumulation rules, averaged throughout the 25 × 25 m scene. CI_a is defined as the 95% confidence interval for two-eared risk determined based on the scene-averaged risk for the $\chi = 0.344$ dose-accumulation rule and under the assumption that both ears have the same risk (effectively, grazing incidence exposure) for all subjects. Values are pulled from simulation with parameters: $N_i = 300$, $R = 7$ m, $\sigma_r = 1$ m, $N_b = 2$ or 14, $1/\lambda = 150$ ms, $\sigma_f = 2$ dB, $\bar{f} = 0$ dB, $K = 40$ dB.

E. Impulse Intensity

The analysis conducted thus far has made use of a derived SELA vs. distance curve (Equation 9) available from (Wang, Burgei, and Zhou 2018) based on recordings of an actual flashbang device. At a distance of 1.8 m (6 feet), Equation 9 computes a SELA for a single impulse of 142.5 dB. According to (Smoorenburg 2003), the SELA of a rifle shot is approximately 37 dB below the peak SPL. Although flashbangs may not match this rule of thumb developed for rifle noise exactly, this puts the estimated peak SPL of the device

in Wang (2018) at approximately 179.5 dB at a distance of 6 feet. As the design range of flashbangs typically targets a peak SPL of 170–180 dB at a distance of 5–6 feet,[11] this device is on the intense side of the typical design range. Therefore, we consider the role of overall impulse intensity through variation of the parameters $\bar{f}$ and σ_f. As a reminder, f is a bias (in decibels) applied additively to the SELA of the sound determined from Equation 9 (Equation 9 is solely a function of the distance of a grid point from a submunition), and it is pulled from a normal distribution with mean $\bar{f}$ and standard deviation σ_f as described in Section 2.

Figure 12 shows the effect of pulse bias on the overall estimate of RSI for the three dose-accumulation rules. The mean risk averaged over the 25 × 25 m scene is 6.9% (3.0, 8.9) for $\bar{f}$ = 5 dB, 4.3% (1.8, 5.6) for $\bar{f}$ = 0 dB, and 2.6% (1.1, 3.4) for $\bar{f}$ = –5 dB. As expected, increasing the average SELA of the impulses increases overall risk, while decreasing the average SELA of the impulses decreases overall risk. But the effect is not symmetric—increasing $\bar{f}$ by 5 dB adds more risk than is removed by an equivalent decrease in $\bar{f}$—because the injury risk curve is a logistic function of the dose, and the slope is steeper on the right side of the typical SELA range of flashbangs than on the left side. There is a risk "floor" on the left side of the logistic-risk curve, since risk can never drop below 0. In this regime, *small increases in SELA have a greater impact on risk than small decreases in SELA.*

Figure 12 also shows that the uncertainty in risk grows as the risk itself grows. The difference between the upper and lower bounds for $\bar{f}$ = 5 dB reaches 9 percentage points at the maximum risk position, more than twice the range seen for $\bar{f}$ = –5 dB.

Manufactured flashbang grenades often exhibit variance in the overall intensity of their impulses as measured at a fixed distance. Manufacturer specification sheets often report their range of device output intensities (peak SPL) at approximately 10 dB (± 5 dB) at a distance of 5–6 feet, although specification sheets reporting variations as large as ± 10 dB exist (Swallow and Sallis-Peterson 2020). We explored the role of the uncertainty in flashbang intensity on the risk predictions by varying the parameter σ_f.

[11] Note that devices that land at the feet of adults will typically be about 5 feet away from the subject's ears; however, individuals may be exposed while seated (for example, if a device is used in an indoor setting) or may be of shorter stature. Proximity to a detonating flashbang also has other (non-auditory) risks. These issues are beyond the scope of the current analysis, but should be considered in a full RSI assessment of a flashbang.

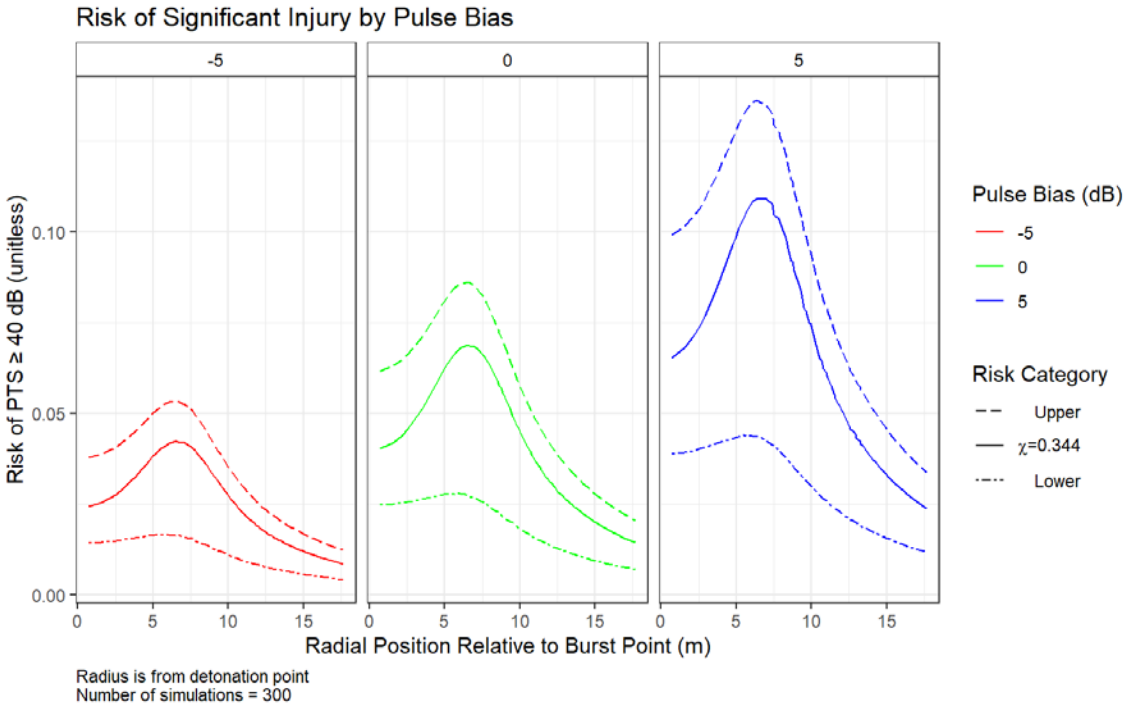

Figure 12. Risk of PTS ≥ 40 dB as a Function of Radial Position Relative to the Burst Point within the 25 × 25 m Simulation Grid for Three Values of Pulse Bias $\bar{f}$. Left (red) lines indicate $\bar{f}$ = –5 dB, center (green) lines indicate $\bar{f}$ = 0 dB, and right (blue) lines indicate $\bar{f}$ = 5 dB. Solid lines estimate risk using the χ = 0.344 dose-accumulation rule. Dashed lines use the upper bound dose-accumulation rule with χ = 1. Dash-dotted lines use the lower bound dose-accumulation rule defined in Equation 10. Parameters for these plots: N_i = 300, R = 7, σ_r = 1 m, $1/\lambda$ = 150 ms, N_b = 11, σ_f = 2 dB, K = 40 dB.

Figure 13 shows that increased uncertainty in the impulse intensity leads to an overall increase in the RSI computed across the full range of radii and dose-accumulation rules. Table 7 summarizes the peak risk and mean risk averaged over the 25 × 25 m scene for simulations with σ_f varied from 1 to 5 dB. The increase in expected risk with increased impulse intensity uncertainty is caused by the asymmetry in the logistic injury-risk curve about the mean in the range of doses representative of flashbangs. As described above, an increase in impulse intensity adds more to the risk than a decrease of the same magnitude removes. As a result, *increased dose variance,* (*with equal* ±dB *values*) *adds to expected risk.*

The effect of impulse intensity standard deviation is larger for the upper bound and χ = 0.344 dose-accumulation rules and smaller for the lower bound rule, as can be seen by comparing the position of the blue lines (σ_f = 5 dB) in Figure 13 relative to the corresponding green and red lines for the three dose-accumulation rules. Although the standard deviation effect does appear for the lower bound dose-accumulation rule, the other dose-accumulation rules allow the effect to accumulate over many impulses, resulting in a large aggregate increase in injury risk when impulse standard deviation increases.

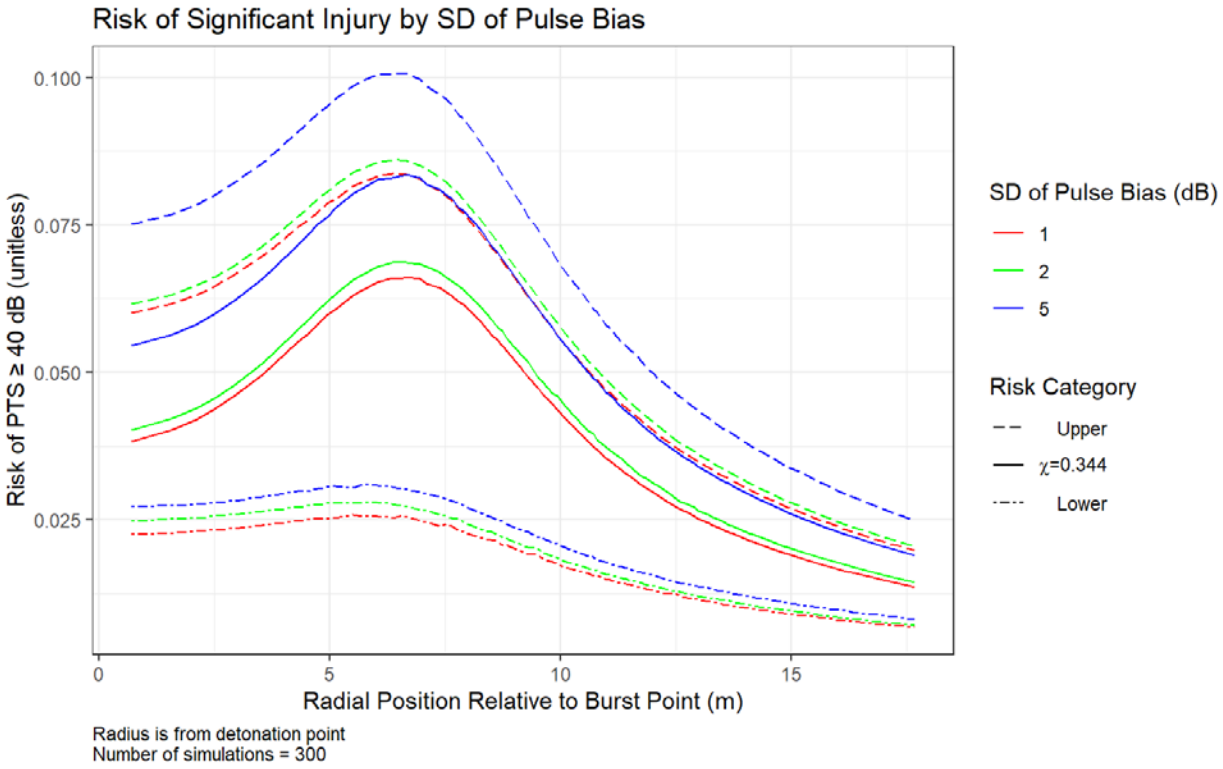

Figure 13. Risk of PTS ≥ 40 dB as a Function of Radial Position Relative to Burst Point within the 25 × 25 m Simulation Grid for Three Values of Pulse Bias Standard Deviation σ_f. Red lines indicate σ_f = 1 dB, green lines indicate σ_f = 2 dB, and blue lines indicate σ_f = 5 dB. Solid lines estimate risk using the χ = 0.344 dose-accumulation rule. Dashed lines use the upper bound dose-accumulation rule with χ = 1. Dash-dotted lines use the lower bound dose-accumulation rule defined in Equation 10. Parameters for these plots: N_i = 300, R = 7, σ_r = 1 m, $1/\lambda$ = 150 ms, N_b = 11, $\bar{f}$ = 0, K = 40 dB.

Table 7. Peak Risk and Scene-Averaged Risk for Differing Pulse Bias Uncertainty σ_f

Pulse Bias Standard Deviation σ_f (m)	Peak Risk			Scene-Averaged Risk		
	Risk (%) (Equation 10)	Risk (%) for χ = 0.344	Risk (%) for χ = 1	Risk (%) (Equation 10)	Risk (%) for χ = 0.344	Risk (%) for χ = 1
1	2.6	6.6	8.4	1.7	4.1	5.4
2	2.8	6.9	8.6	1.8	4.3	5.6
5	3.1	8.4	10.1	2.0	5.3	6.6

Parameters for these simulations: N_i = 300, R = 7 m, σ_r = 1 m N_b = 11, $1/\lambda$ = 150 ms, $\bar{f}$ = 0 dB, K = 40 dB.

These results indicate the importance of accounting for the standard deviation of a device's output when computing expected RSI. As we have seen, it is not enough to simply compute the risk associated with the mean device output. Instead, *aggregate RSI calculations must factor in the role of device output variation because the asymmetric nature of the injury-risk curve in the flashbang dose regime causes increased expected risk*

for devices with wider output uncertainty ranges. In the example shown here, accounting for uncertainty of ±5 dB in device output leads to an increased mean expected RSI in the 25 × 25 m scene of more than 1 percentage point and an increase in peak RSI of nearly 2 percentage points relative to a simulation where device output is constrained (±1 dB). This is a ~30% relative increase in the computed expected risk, determined by accounting for a variation in the device output of only a few decibels. Although the effect is not as large as that of a change in the actual mean device output represented by $\bar{f}$, it is still substantial enough to distinguish the expected RSI of devices produced by different manufacturers that specify different uncertainty ranges for the same mean output.

F. Risk Threshold *K*

Our analysis thus far has focused on a significant injury threshold of 40 dB because it is the current standard used by the DoD. However, past analysis has suggested that a lower threshold of 25 dB may be a reasonable alternative for defining significant PTS (King and Cazares 2015). Therefore, we review the role of the choice of threshold on overall risk profiles by varying the parameter *K*.

Figure 14 displays heat maps of injury risk in the 25 × 25 m scene computed for the two injury risk thresholds and three dose-accumulation rules. The mean risk averaged over the 25 × 25 m scene is 4.3% (1.8, 5.6) for K = 40 dB, and 9.4% (4.0, 12.2) for K = 25 dB. For peak risk, these ranges are: 6.9% (2.8, 8.6) for K = 40 dB, and 14.9% (5.9, 18.3) for K = 25 dB.

Both the computed risk and the range of uncertainty due to the dose-accumulation rule more than double when the threshold of significance K is dropped from 40 to 25 dB, because when K is set to 40 dB, many impulses that land far from the subject have SELA values that fall in the flat (effectively zero risk) portion of the logistic injury-risk curve. But when K is set to 25 dB, these same impulses now have a small, but appreciable risk of injury. Visually, this causes the heat map of overall risk to become brighter and more completely fill the 25 × 25 m scene, as shown in Figure 14. Practically, this causes the computed overall risk at any given position to increase substantially.

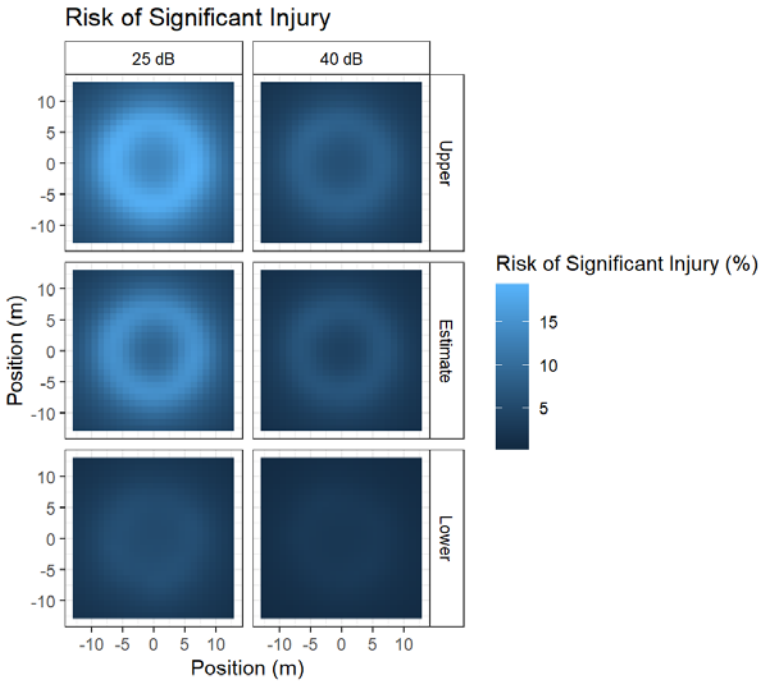

Figure 14. Heat Maps of Average Risk of PTS ≥ 25 dB (left) and PTS ≥ 40 dB (right) as a Function of Position with Three Methods of Computing Dose Accumulation (top = upper bound method, middle = χ = 0.344 dose-accumulation rule, bottom = lower bound). Averages are taken at each position over all N_i = 300 Monte Carlo simulations in a given run. Parameters for these plots: R = 7 m, σ_r = 1 m, N_b = 11, $1/\lambda$ = 150 ms, σ_f = 2 dB, $\bar{f}$ = 0 dB.

In addition to varying K alone, a few additional simulations were conducted to explore the effect of variation in σ_f or $\bar{f}$ for K = 25 dB. The mean risks and peak risks for these conditions can be found for simulations 24–27 in Table B-1 and Table B-2, respectively. The results are also plotted in Figure 15 and Figure 16. In general, the trends observed for K = 40 dB and Section 3.E persist.

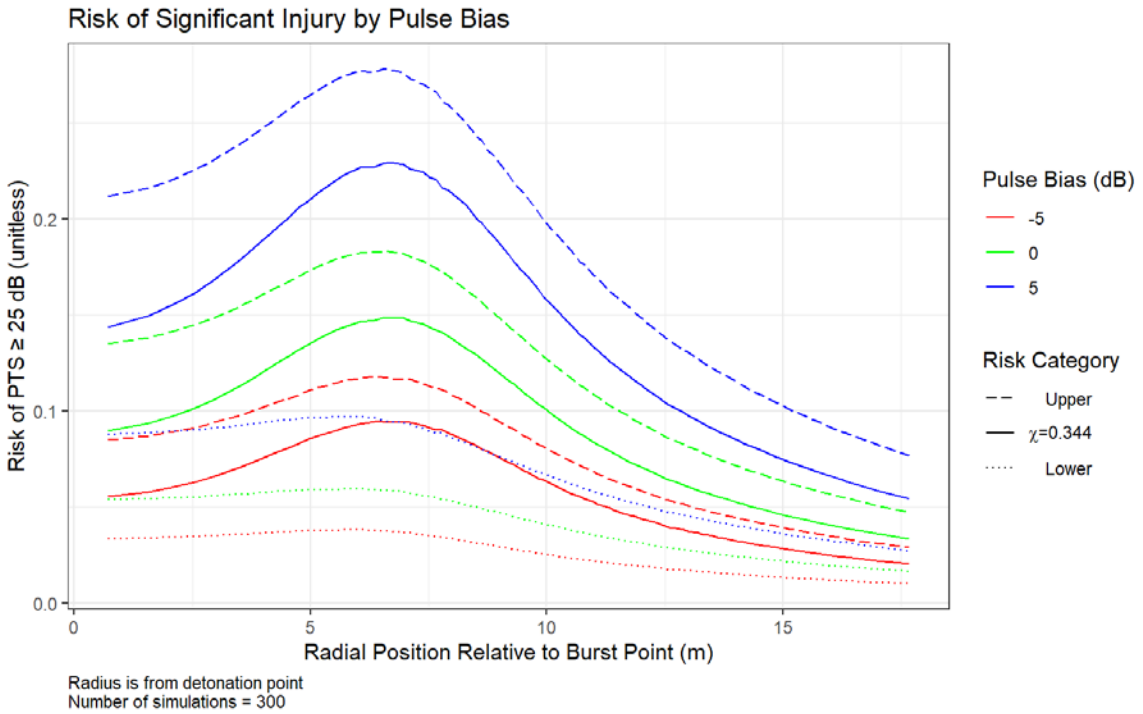

Figure 15. Risk of PTS ≥ 25 dB as a Function of Radial Position Relative to the Burst Point within the 25 × 25 m Simulation Grid for Three Values of Pulse Bias $\bar{f}$. Red lines indicate $\bar{f}$ = –5 dB, green lines indicate $\bar{f}$ = 0 dB, and blue lines indicate $\bar{f}$ = 5 dB. Solid lines estimate risk using the χ = 0.344 dose-accumulation rule. Dashed lines use the upper bound dose-accumulation rule with χ = 1. Dotted lines use the lower bound dose-accumulation rule defined in Equation 10. Parameters for these plots: N_i = 300, R = 7, σ_r = 1 m, $1/\lambda$ = 150 ms, N_b = 11, σ_f = 2, K = 25 dB.

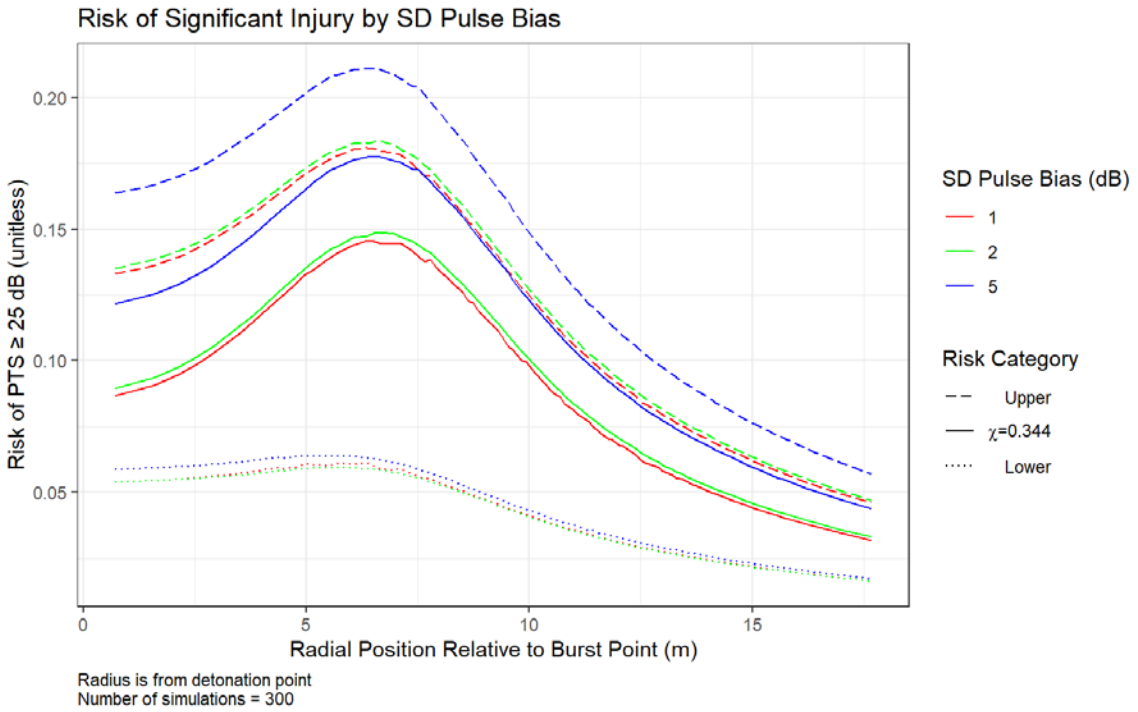

Figure 16. Risk of PTS ≥ 25 dB as a Function of Radial Position Relative to the Burst Point within the 25 × 25 m Simulation Grid for Three Values of Pulse Bias Standard Deviation σ_f. Red lines indicate σ_f = 1 dB, green lines indicate σ_f = 2 dB, and blue lines indicate σ_f = 5 dB. Solid lines estimate risk using the χ = 0.344 dose-accumulation rule. Dashed lines use the upper bound dose-accumulation rule with χ = 1. Dotted lines use the lower bound dose-accumulation rule defined in Equation 10. Parameters for these plots: N_i = 300, R = 7, σ_r = 1 m, $1/\lambda$ = 150 ms, N_b = 11, $\bar{f}$ = 0, K = 25 dB.

In particular, these figures again show that greater uncertainty in the flashbang intensity (increased σ_f) leads to increased average risk in the scene and increased peak risk. At the K = 25 dB threshold, increasing σ_f from 1 to 5 dB increases the average risk in the scene by 2.5 percentage points (27% relative to the σ_f = 1 value of 9.2%), while the same change in σ_f increases the peak risk by 3.2 percentage points (22% of the σ_f = 1 value). Contrasting this to the relative changes at K = 40 dB (29% and 27%, respectively), we see that the degree of asymmetry at K = 25 dB is slightly reduced, since the doses fall closer to (though still below) the inflection point of the logistic curve for K = 25 dB than they do for the K = 40 dB curve. Despite this, the absolute change in risk for K = 25 dB is larger for these effects than it was for K = 40 dB, even though the relative change is smaller. This demonstrates that accounting for effects such as uncertainty in device output remains important at this lower K value.

Were we to reduce K further, or increase the flashbang output by substantially increasing $\bar{f}$, we would eventually reach a point where increased uncertainty in σ_f actually led to decreased estimated risk. However, flashbang designs do not typically produce doses near the inflection point for K = 40 dB or K = 25 dB. The inflection point occurs when risk

is equal to 50% *for a single ear*. Even our $\bar{f}$ = 5 dB, K = 25 dB simulation, which simulates a multi-impulse flashbang with an output well above the standard for most flashbangs, only reaches a peak RSI (with the upper bound dose-accumulation rule) for injury *to at least one ear* of 27.8% at the highest risk radial position. While this is a large risk, it is well below the inflection point in the logistic curve, meaning that the trends described in this section remain valid.

4. Conclusion

In this report we have explored key factors in the estimation of risk of significant injury for multi-impulse, area-distributed flashbang exposures that occur at time scales of relevance to the acoustic reflex. We have also estimated uncertainty in expected risk in such exposures by applying bounding assumptions on the dose-accumulation rules and varied the parameters of a mortar device that distributes submunitions over an area to explore tradeoffs between device design and risk.

We explored the uncertainty in estimated injury risk for this type of exposure by applying a bounding-analysis approach to dose accumulation. The lower bound risk was estimated by assuming a 100% protective acoustic reflex; the upper bound of risk was estimated by applying the equal-energy criterion (referred to in this report as the $\chi = 1$ rule), which permits no trading for intensity vs. number of impulses in computing injury risk. Our analysis demonstrated that the uncertainty in dose-accumulation rule can lead to large uncertainties in expected RSI, particularly when the number of impulses is high or the overall risk of injury is high. Furthermore, we provided examples in this analysis where the uncertainty in expected risk caused by the dose-accumulation rule is of similar scale to the uncertainty in individual exposure risk at a given position due to the pattern of munitions. In fact, we found that the relative size of uncertainty ranges related to the pattern of submunitions *decreased* with increased number of submunitions, while the relative size of uncertainty related to the dose-accumulation rule increased. We also found that the risks computed in the highest risk region of the exposure scene were more sensitive to the pattern of submunitions than those computed in the low-risk regions of the scene. Overall, our analysis shows that uncertainty about the role of the acoustic reflex in protecting targets from significant injury becomes more important when multi-impulse tactics and devices are employed in short (second-scale) time intervals.

Our analysis also covered the effects of variations in design parameters for our example mortar device. Table 8 summarizes the results. In particular, we found that larger burst radii (distributing submunitions over a wider area) have the effect of reducing the expected peak risk while spreading risk more evenly within the 25 × 25 m zone. Increased uncertainty in burst radius causes a slight decrease in the radial position (relative to the mortar burst point) of maximum risk and a slight depression in the maximum overall risk, further broadening risk across the exposed area and increasing the average risk in the scene slightly. Both the peak risk and the average risk in the scene increase as a function of the number of submunitions N_b for both $\chi = 0.344$ and $\chi = 1$ (upper bound) dose-accumulation

rules. The effect of the inter-pulse interval on computed risk was small relative to other effects explored in this analysis.

Table 8. Summary of Effects on Peak and Scene-Averaged RSI of Varying Parameters in Design of a Mortar Device that Distributes Submunition Flashbangs Over an Area

Action	Effect on Peak Risk	Effect on Scene-Average Risk
Increase burst radius R	Decrease (Moderate)	Non-monotonic, depends on scene size
Increase burst radius uncertainty σ_r	Decrease (Minor)	Increase (Minor)
Increase average IPI λ	Decrease (Minor)	Decrease (Minor)
Increase N_b	Increase (Major)	Increase (Major)
Increase $\bar{f}$	Increase (Major)	Increase (Major)
Increase σ_f	Increase (Moderate)	Increase (Moderate)

We also found that due to the asymmetry in the logistic injury-risk curve in the typical flashbang dose regime, small increases in device output (in A-weighted decibels) have a greater impact on risk than small decreases. For the same reason, increased device output variance, although with equal ±dB values, has the effect of increased expected and peak injury risk in the scene. These results illustrate the need for aggregate RSI calculations to factor in the role of device output variation and not simply compute risk based on the mean or expected device output.

Both the computed risk and the range of uncertainty due to the dose-accumulation rule more than double when the threshold of significance is dropped from 40 to 25 dB. The asymmetry of the logistic-regression curve in the flashbang dose regime is slightly reduced for this change as well. The difference of 15 dB in the threshold of significant injury makes a substantial impact on estimates of risk. These thresholds should be carefully considered when trying to understand the human auditory effects of flashbangs.

While we have explored the role of device parameters on the *injury risks* associated with multi-impulse flashbangs, the role of these same parameters in contributing to device effectiveness should also be explored to identify methods of reducing injury risk while maintaining or improving device effectiveness. Open questions exist about how the parameters of multi-impulse flashbang exposures affect the behavior of human targets. New models are needed to connect parameters such as those explored in this study to behavioral outcomes, in addition to injury risks.

These results point to choices that may be available in the design of a mortar- and submunition-type flashbang to tune injury risk profiles. For example, if the designer's goal is to reduce overall average risk in an area, changes such as decreasing the uncertainty in

sound-output intensity may be appropriate, in addition to more obvious actions such as decreasing the number of submunitions or the expected sound output intensity of a given submunition. In contrast, to decrease the peak risk (i.e., to decrease the risk of very serious injury while potentially accepting slightly increased average RSI), actions such as increasing the burst radius or the burst-radius uncertainty or decreasing the individual impulse-intensity uncertainty may be appropriate.

This report offers a method (the bounding approach) that can be extended to other device designs or deployment concepts (e.g., using multiple devices instead of multi-impulse single devices) to estimate the size of uncertainties related to the choice of dose-accumulation rule. The use of Monte Carlo simulation to explore a range of operational scenarios is also a feature of this analysis that can be adapted to different types of environments (e.g., reverberant vs. open) or operational concepts.

We did not explore the role of tympanic membrane rupture (TMR) in contributing to RSI calculations; however, TMR is another significant injury to the auditory system that can be caused by flashbangs. Within the design space of most flashbangs, the risk of TMR from a single impulse is below the risk of PTS ≥ 40 dB and well below the risk of PTS ≥ 25 dB. Few data exist on the accumulated or multi-impulse exposure effects on TMR risk, a shortcoming that may be possible to remedy through a mix of animal subject experimentation and biofidelic modeling. Such biofidelic modeling would ideally also include the nonlinear action of the acoustic reflex and other components of the auditory system, using parameters derived from experimental data such as those collected by (Deiters et al. 2019; McGregor et al. 2018; Greene et al. 2017, 2018).

The visual effects of flashbangs, the effects of blast overpressure on the body, and direct contact with components of flashbangs during or shortly after detonation may cause non-auditory significant injuries not covered in this work. Except for visual and overpressure effects, most of these injuries (e.g., burns or shrapnel injuries) are of most concern when a flashbang lands or detonates extremely close to a target. In a full analysis of RSI from a multi-submunition device, the possibility of these injuries should be included. Ideally, a Monte Carlo–style simulation similar to the one described in this report would be used to generate patterns of submunitions for which the risk of all potential injury types is computed at once within a given iteration. This would prevent calculations of RSI from neglecting the likely co-occurrence of certain injury types that are only likely in extreme proximity to individual submunitions.

Flashbangs are also used in combination with lethal weapons in a number of operational scenarios, for example, in combat room-clearing operations where a flashbang may be deployed followed by rifle fire. This analysis does not cover the combined auditory effects of these two sources of impulse noise, but modeling concepts for such combinations could be of use, particularly for understanding occupational risks to soldiers.

This analysis provides a methodology for exploring both the role of device parameters and the choice of dose-accumulation rule in estimating RSI and associated uncertainty for multi-impulse exposures with short (< 1 s) inter-pulse intervals. This analysis can describe how decisions about the design and operational usage of flashbangs (such as how many devices to use or where to aim them relative to a group of people) affect potential risk patterns in an area. To make full use of this analysis, similar work exploring the role of such parameters on the human effectiveness of devices is also required.

Appendix A.
Radial Risk Plots

This appendix discusses some of the nuances associated with plotting data using radial risk plots, as is frequently done throughout this report. Radial risk plots allow easier visual comparison of risks computed for simulations with different parameters. Such plots take advantage of the cylindrical symmetry observed for the 300-iteration risk maps, and average risk for points of equivalent radius in the scene. This has the effect of reducing some noise and obscuring some of the angular variation that is observed in full risk maps due to angle-of-incidence effects. However, as shown in this appendix, none of the trends observed or discussed in the main report are expected to be affected by this radial averaging.

Figure A-1 shows the number of points used for each radial position to compute the risk as a function of radius based on the risk maps. As shown, the vast majority of radial positions, covering nearly the full range of radii contained in the simulated 25 × 25 m square, use eight points. A few radial positions use only 4 data points, while some use 12 or 16, and 1 radial position (12.7 m) uses 24. These multiples of 4 are a consequence of the discretized square grid of 625 points with 1 m spacing used to compute the risk maps. As seen in the main report, radial risk plots typically show smooth progressions of risk as a function of radius. These data indicate little systematic variation in the precision or accuracy of risk computed as a function of radius in the report. In other words, the values computed for risk at smaller radii are as reliable as the values computed for risk at larger radii.

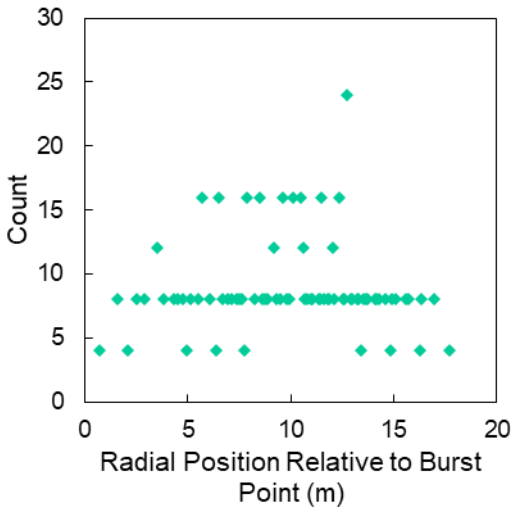

Figure A-1. Count of Number of Points from Risk Maps Used to Compute Risk in Radial Risk Plots for Each Radial Value

Note that for radial risk plots, the area *rdr* of the scene that corresponds to a given radius *r* increases with increasing radius *r*. Integrating a radial risk function $p(r)$ to compute average risk in an area would need to use the Jacobean *rdr* to account for the use of polar coordinates. In other words, averaging risk throughout the 25 × 25 m scene weights risks at larger radial positions more heavily.

An alternative to the radial risk plot is the line trace. Rather than averaging risk for all radially equivalent positions in the scene, a line trace simply plots risk as a function of *x* or *y* at fixed *y* or *x*, respectively. Figure A-2, Figure A-4, and Figure A-3 show some example line traces. These line traces are pulled from the same data sets used to generate Figure 6, Figure 10, and Figure 13, respectively, and represent 10 of the 21 300-iteration simulations analyzed in the report. These line traces average the results of $y = \pm 0.5$ m to represent a track through the center of the scene.

As expected, the figures slow slightly more noise in the values at each position than is seen in their corresponding radial figures that average over more than two points. Even so, the trends in risk across the varied parameters are consistent with what was observed in the radial plots, and the quantitative risk values are also consistent, though with slight deviations.

A slight degree of left-right asymmetry is observed for some of the line traces. This asymmetry is most clearly observed in the $N_b = 2$, 5, and 14 traces in Figure A-3, where the difference in the height of the left and right peaks in the line traces reaches up to 0.004 in the worst case for the $\chi = 1$ dose-accumulation rule. For the $\chi = 0.344$ rule, this deviation in peak height reduces to about 0.002, which is comparable to the uncertainty expected for risk as a function of radius based on the convergence study conducted to select the number of Monte Carlo iterations. Note that the traces shown in these figures do not show

consistent asymmetry in one direction or the other—sometimes the left peak is taller, sometimes the right peak is taller, and often the two peaks appear to be the same height. These left-right asymmetries in some of the line traces are explained by small quantities of noise in risk as a function of position within the risk maps. The radial risk plots smooth this source of noise by averaging across several points in the scene. These observations are not expected to have any effect on the report's conclusions.

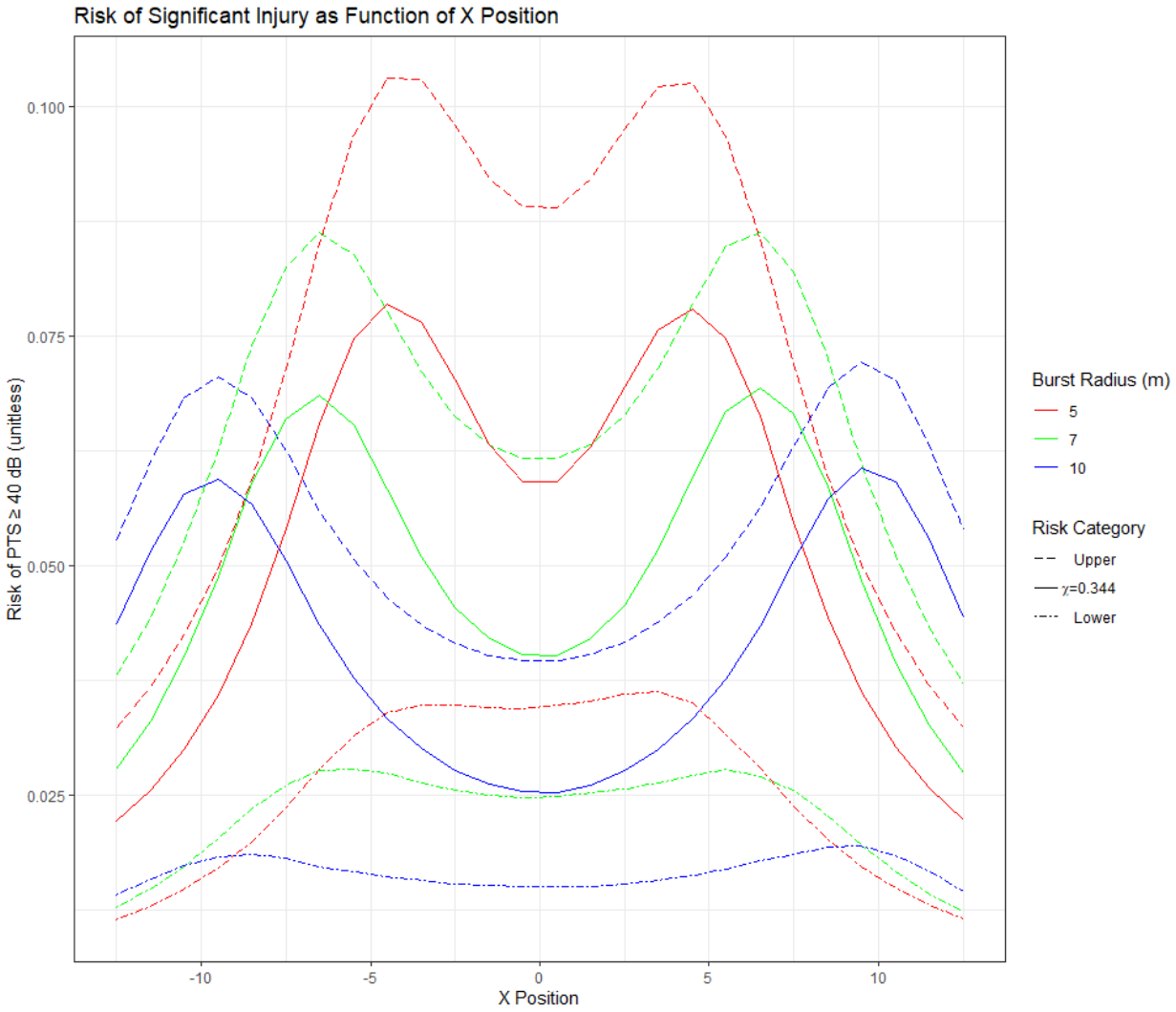

Figure A-2. Risk of PTS ≥ 40 dB as a Function of *x* Position for Fixed *y* = 0 (average of values at *y* = ±0.5 m) within the 25 × 25 m Simulation Grid for Three Values of Burst Radius *R*. Red lines indicate *R* = 5 m, green lines indicate *R* = 7 m, and blue lines indicate *R* = 10 m. Solid lines estimate risk using the $\chi = 0.344$ dose-accumulation rule. Dashed lines use the upper bound dose-accumulation rule with $\chi = 1$. Dash-dotted lines use the lower bound dose-accumulation rule defined in Equation 10. Parameters for these simulations: $N_i = 300$, $\sigma_r = 1$ m, $N_b = 11$, $1/\lambda = 150$ ms, $\sigma_f = 2$ dB, $\bar{f} = 0$ dB, $K = 40$ dB.

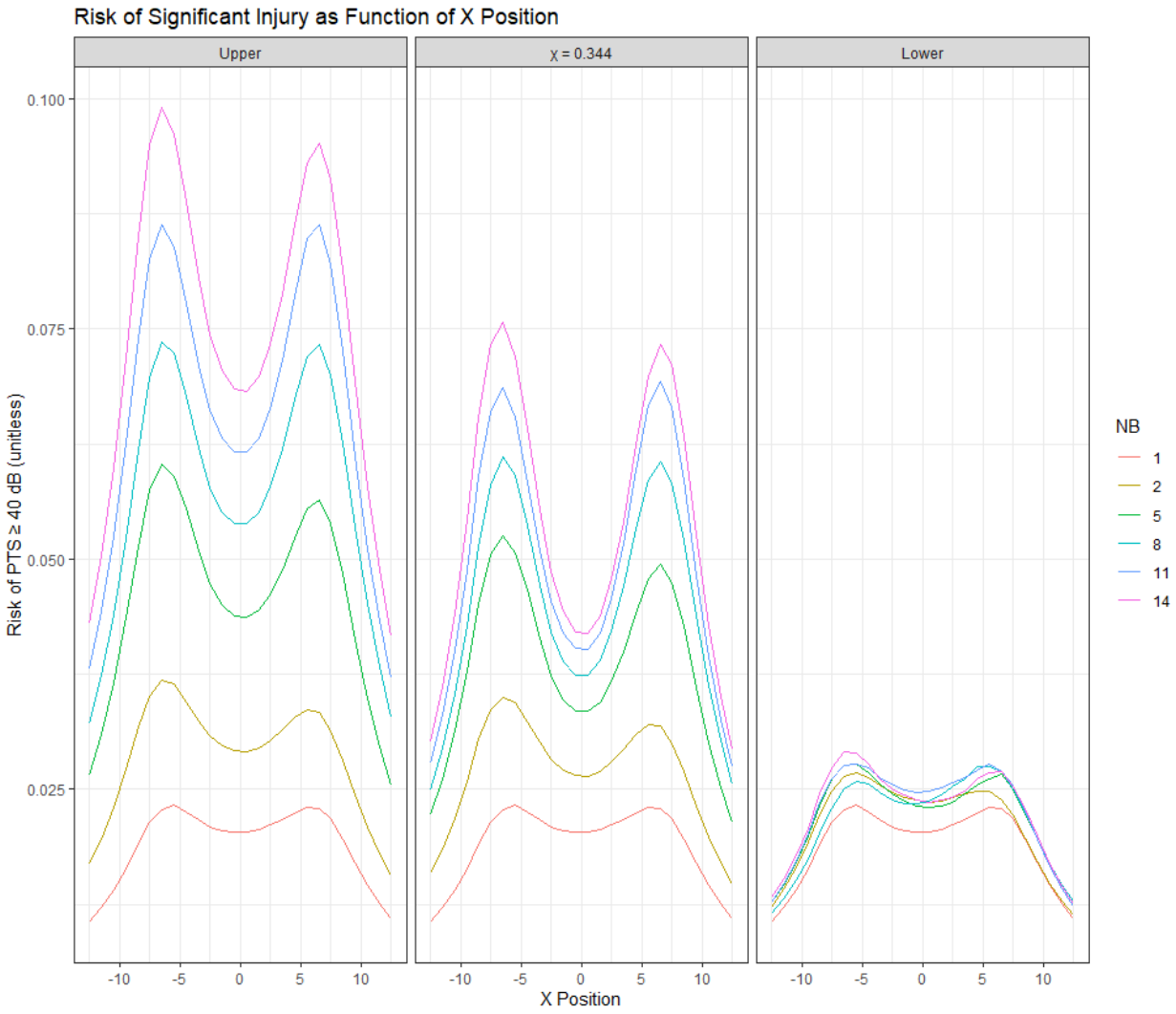

Figure A-3. Risk of PTS ≥ 40 dB as a Function of *x* Position for Fixed *y* = 0 within in the 25 × 25 m Scene. Line color indicates the number of submunitions N_b. Left panel estimates risk using the χ = 0.1 dose-accumulation rule. Middle panel uses the χ = 0.344 dose-accumulation rule. Right panel uses the lower bound dose-accumulation rule defined by Equation 10. Parameters for these plots: N_i = 300, R = 7, σ_r = 1 m, $1/\lambda$ = 150 ms, σ_f = 2 dB, $\bar{f}$ = 0 dB, K = 40 dB.

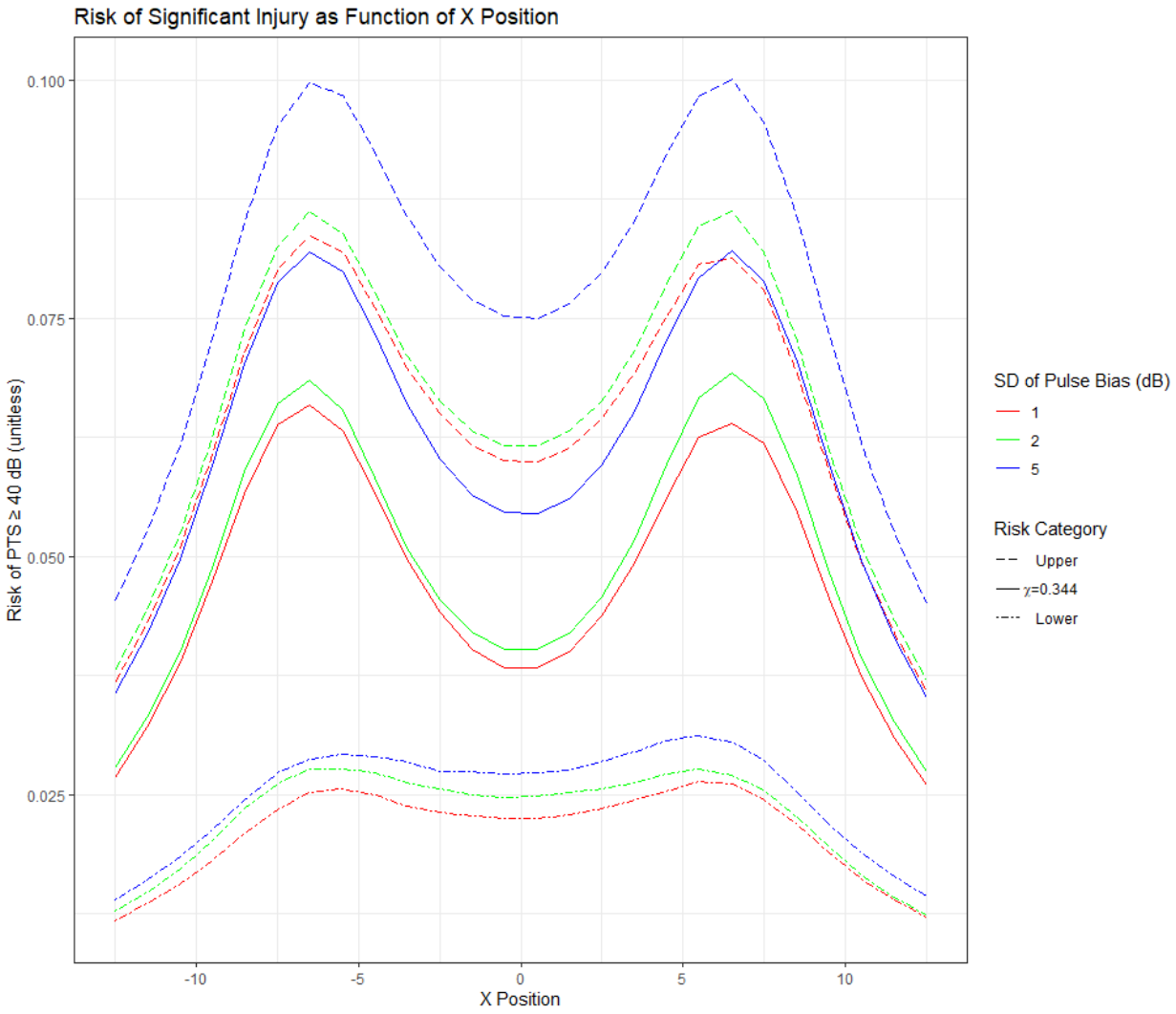

Figure A-4. Risk of PTS ≥ 40 dB as a Function of x Position for Fixed y = 0 within the 25 × 25 m Simulation Grid for Three Values of Pulse Bias Standard Deviation σ_f. Red lines indicate σ_f = 1 dB, green lines indicate σ_f = 2 dB, and blue lines indicate σ_f = 5 dB. Solid lines estimate risk using the χ = 0.344 dose-accumulation rule. Dashed lines use the upper bound dose-accumulation rule with χ = 1. Dash-dotted lines use the lower bound dose-accumulation rule defined in Equation 10. Parameters for these plots: N_i = 300, R = 7, σ_r = 1 m, $1/\lambda$ = 150 ms, N_b = 11, $\bar{f}$ = 0, K = 40 dB.

Appendix B.
Tables of Simulation Results

Table B-1. Mean Risk of Injury Computed for the 25 m x 25 m Grid (%)

Simulation Number	Key Varied Parameter(s)	Equation 8 rule	χ = 0.344 rule	χ = 1 rule
1	N_i = 1	1.48	4.66	5.95
2	N_i = 10	1.74	4.40	5.73
3	N_i = 30	1.79	4.28	5.62
4	N_i = 50	1.87	4.33	5.61
5	N_i = 100	1.81	4.21	5.53
6	*DEFAULTS*	1.84	4.27	5.56
7	N_i = 1000	1.79	4.26	5.57
8	R = 5 m	1.8	3.9	5.4
9	R = 10 m	1.6	4.4	5.5
10	$\sigma_r = 0.5$ *m*	1.8	4.2	5.5
11	$\sigma_r = 2$ *m*	1.7	4.3	5.6
12	N_b = 1	1.5	1.5	1.5
13	N_b = 2	1.8	2.2	2.3
14	N_b = 5	1.8	3.2	3.8
15	N_b = 8	1.8	3.9	4.8
16	N_b = 14	1.8	4.6	6.2
17	$1/\lambda$ = 100 ms	1.9	4.3	5.6
18	$1/\lambda$ = 200 ms	1.7	4.2	5.5
19	σ_f = 1 dB	1.7	4.1	5.4
20	σ_f = 5 dB	2.0	5.3	6.6
21	$\overline{f}$ = -5 dB	1.1	2.6	3.4
22	$\overline{f}$ = 5 dB	3.0	6.9	8.9
23	K = 25 dB	4.0	9.4	12.2
24	K = 25 dB, σ_f = 1 dB	4.1	9.2	12.0
25	K = 25 dB, σ_f = 5 dB	4.3	11.7	14.3
26	K = 25 dB, $\overline{f}$ = -5 dB	2.5	5.9	7.7
27	K = 25 dB, $\overline{f}$ = 5 dB	6.6	14.9	18.9

*The key varied parameters in a simulation are the parameters that deviate from the default set defined in Table 1. Risks reported in this table are computed as risk of PTS ≥ 40 dB unless K is specified as a key varied parameter, in which case risk is computed as risk of PTS ≥ 25 dB.

Table B-2. Risk of Injury Computed at the Maximum Risk Radius (%)

Simulation Number	Key Varied Parameter(s)	Equation 8 rule	χ = 0.344 rule	χ = 1 rule
1	N_i = 1	2.72	7.46	8.98
2	N_i = 10	2.71	7.24	9.04
3	N_i = 30	2.72	6.97	8.74
4	N_i = 50	2.80	6.97	8.66
5	N_i = 100	2.74	6.97	8.74
6	*DEFAULTS*	2.79	6.87	8.60
7	N_i = 1000	2.70	6.88	8.61
8	R = 5 m	3.6	7.8	10.3
9	R = 10 m	1.9	5.9	7.1
10	σ_r = *0.5 m*	2.7	7.1	8.8
11	σ_r = *2 m*	2.5	6.4	8.1
12	N_b = 1	2.3	2.3	2.3
13	N_b = 2	2.6	3.4	3.5
14	N_b = 5	2.7	5.1	5.8
15	N_b = 8	2.7	6.2	7.4
16	N_b = 14	2.7	7.4	9.7
17	$1/\lambda$ = 100 ms	2.9	6.9	8.6
18	$1/\lambda$ = 200 ms	2.6	6.7	8.5
19	σ_f = 1 dB	2.6	6.6	8.4
20	σ_f = 5 dB	3.1	8.4	10.1
21	$\overline{f}$ = -5 dB	1.7	4.2	5.3
22	$\overline{f}$ = 5 dB	4.4	10.9	13.6
23	K = 25 dB	5.9	14.9	18.3
24	K = 25 dB, σ_f = 1 dB	6.1	14.6	18.1
25	K = 25 dB, σ_f = 5 dB	6.4	17.8	21.1
26	K = 25 dB, $\overline{f}$ = -5 dB	3.8	9.5	11.8
27	K = 25 dB, $\overline{f}$ = 5 dB	9.7	22.9	27.8

*The key varied parameters in a simulation are the parameters that deviate from the default set defined in Table 1. Risks reported in this table are computed as risk of PTS ≥ 40 dB unless K is specified as a key varied parameter, in which case risk is computed as risk of PTS ≥ 25 dB.

Table B-3. Radial Position of Maximum Injury Risk (m)

Simulation Number	Key Varied Parameter(s)	Equation 8 rule	χ = 0.344 rule	χ = 1 rule
1	N_i = 1	6.36	7.52	7.52
2	N_i = 10	4.95	7.11	6.36
3	N_i = 30	5.52	6.67	6.67
4	N_i = 50	5.52	7.11	6.36
5	N_i = 100	5.70	6.36	6.36
6	*DEFAULTS*	5.70	6.52	6.36
7	N_i = 1000	5.52	6.67	6.52
8	R = 5 m	3.5	4.5	4.3
9	R = 10 m	9.3	9.8	9.6
10	σ_r = *0.5 m*	6.0	6.7	6.7
11	σ_r = *2 m*	4.5	6.4	6.4
12	N_b = 1	5.5	5.5	5.5
13	N_b = 2	4.9	6.4	6.0
14	N_b = 5	6.0	6.5	6.5
15	N_b = 8	6.4	6.4	6.4
16	N_b = 14	5.7	6.4	6.4
17	1/λ = 100 ms	5.5	6.7	6.5
18	1/λ = 200 ms	6.0	6.5	6.5
19	σ_f = 1 dB	5.5	6.7	6.4
20	σ_f = 5 dB	5.7	6.7	6.7
21	$\overline{f}$ = -5 dB	5.5	6.5	6.5
22	$\overline{f}$ = 5 dB	5.5	7.0	6.4
23	K = 25 dB	5.7	6.7	6.7
24	K = 25 dB, σ_f = 1 dB	6.4	6.4	6.4
25	K = 25 dB, σ_f = 5 dB	5.7	6.5	6.5
26	K = 25 dB, $\overline{f}$ = -5 dB	6.0	6.4	6.4
27	K = 25 dB, $\overline{f}$ = 5 dB	5.7	6.7	6.7

*The key varied parameters in a simulation are the parameters that deviate from the default set defined in Table 1. Risks reported in this table are computed as risk of PTS ≥ 40 dB unless K is specified as a key varied parameter, in which case risk is computed as risk of PTS ≥ 25 dB.

Appendix C.
Piecewise-Continuous Confidence Intervals for Auditory 4.5

Auditory 4.5 has built-in confidence intervals described in the Auditory 4.5 API documentation (Adkins et al. 2019). However, IDA's analysis of the Auditory 4.5 model determined that uncertainty in the linear shift used to translate from chinchilla to human data was not accounted for in creating these confidence intervals (Swallow and Kramer 2019). Further, IDA confirmed that this shift should be overlaid on confidence intervals produced from initial curve fitting of the large chinchilla data set, rather than added to them. The result is piecewise-continuous confidence intervals for injury risk at different thresholds of PTS. This appendix shows how these piecewise-continuous confidence intervals are derived.

Auditory 4.5 Risk Estimation and Confidence Intervals

Auditory 4.5 estimates injury risk using a series of equations described in the Auditory 4.5 API documentation and summarized here.

The model estimates risk of injury using a logistic regression:

$$P(PTS \geq K[dB]) = \frac{e^L}{1+e^L}.$$

L is computed based on the ordered logistic-regression coefficients determined for Auditory 4.5:

$$L = b_0 + b_1 A\ .$$

The dose A, which is in units of decibels, is defined with several correction terms:

$$A = SELA + B - C - D\ .$$

Here, *SELA* is the A-weighted sound exposure level computed for a single impulse, B is a correction for the number of impulses, C is the chinchilla-to-human error correction (set at 28 dB in Auditory 4.5), and D is the angle-of-incidence correction drawn from Auditory 4.5's lookup tables. IDA's prior analysis determined that the 95% confidence interval for the value of the shift in estimated dose for humans C is 27–33 dB, or a range of +5/–1 dB relative to the built-in value of 28 dB in Auditory 4.5.

The confidence intervals available in Auditory 4.5 are computed by substituting a modified dose L_{CI} for L into the logistic-regression equation:

$$L_{CI} = L \pm 1.96\sqrt{(\sigma_{00}^2 + 2\sigma_{01}^2 A + \sigma_{11}^2 A^2)}\,.$$

The parameters σ_{00}^2, σ_{01}^2, σ_{11}^2, b_0, and b_1 are reported for each threshold level K in the Auditory 4.5 API documentation.

Computing Piecewise-Continuous Confidence Intervals

To determine the piecewise-continuous confidence interval for a given threshold level, we must compute the points at which the corrections to L based on the two sources of uncertainty are equivalent. In other words, we must solve the equation:

$$1.96\sqrt{(\sigma_{00}^2 + 2\sigma_{01}^2 A + \sigma_{11}^2 A^2)} = b_1 \eta\,.$$

Here, η is either 5 or 1, corresponding to the (+5, –1) dB confidence interval for C. This amounts to solving a quadratic equation in A:

$$\sigma_{11}^2 A^2 + 2\sigma_{01}^2 A + \sigma_{00}^2 - (\frac{b_1 \eta}{1.96})^2 = 0\,,$$

$$A = \frac{-2\sigma_{01}^2 \pm \sqrt{(4\sigma_{01}^4 - 4\sigma_{11}^2(\sigma_{00}^2 - (\frac{b_1 \eta}{1.96})^2))}}{2\sigma_{11}^2}\,,$$

$$A = \frac{-\sigma_{01}^2 \pm \sqrt{(\sigma_{01}^4 - \sigma_{11}^2(\sigma_{00}^2 - (\frac{b_1 \eta}{1.96})^2))}}{\sigma_{11}^2}\,.$$

For PTS ≥ 40 dB, we have the following values:

b_1 = 0.1014765

σ_{00}^2 = 1.1506542

σ_{01}^2 = -0.0092653

σ_{11}^2 = 0.0000753

For η = 5, the roots of the equation are A = 150.4 dB and 95.7 dB.

For η = 1, the roots of the equation are imaginary.

This means that for η = 1, the uncertainty in estimated risk of injury due to chinchilla-human translation is always within the existing upper-bound-risk confidence interval (which sits to the left of the injury correlate) for PTS ≥ 40 dB. However, for η = 5, the uncertainty due to chinchilla-human translation is greater than the uncertainty due to initial curve fitting for all doses A between 95.7 and 150.4 dB. In other words, the confidence intervals for K = 40 dB are given by:

$$L_{CI}^{+} = L + 1.96\sqrt{(\sigma_{00}^2 + 2\sigma_{01}^2 A + \sigma_{11}^2 A^2)}\,,$$

and

$$L_{CI}^{-} = L - 1.96\sqrt{(\sigma_{00}^2 + 2\sigma_{01}^2 A + \sigma_{11}^2 A^2)}, A < 95.7 \text{ dB or } A > 150.4 \text{ dB},$$

$$L_{CI}^{-} = L - 5b_1, 150.4 > A > 95.7 \text{ dB}.$$

When we instead set the threshold K to 25 dB, we have the following coefficients:

b_1 = 0.1014765

σ_{00}^2 = 1.1263525

σ_{01}^2 = -0.00918256

σ_{11}^2 = 0.0000753

This results in a crossover range of 93.6 to 150.3 dB for the L_{CI}^{-} confidence interval for PTS $\geq$ 25 dB.

Appendix D.
References

Adkins, Mark, Kevin Ho, Anthony Iyoho, and Philemon Chan. 2019. "Auditory Injury Model 4.5 API Documentation." L3 Applied Technologies.

Chan, Philemon C, Kevin H Ho, Kit K Kan, James H Stuhmiller, and Maria A Mayorga. 2001. "Evaluation of Impulse Noise Criteria Using Human Volunteer Data." *The Journal of the Acoustical Society of America* 110. http://asa.scitation.org/doi/abs/10.1121/1.1391243.

Chan, Philemon, Kevin Ho, and Allen F. Ryan. 2016. "Impulse Noise Injury Model." *Military Medicine* 181: 59.

Chan, Philemon, Kevin Ho, and Brissi Zagadou. 2018. "Incident Angle Correction Algorithm for Impulse Noise Injury Assessment." *Military Medicine* 183: 252–61.

Church, G. T., and E. A. Cudahy. 1984. "The Time Course of the Acoustic Reflex." *Ear and Hearing* 5 (4): 235–42.

Coles, R. Ross A., Georges R. Garinther, David C. Hodge, and Christopher G. Rice. 1967. "Criteria for Assessing Hearing Damage Risk from Impulse-Noise Exposure." HEL-TM-13-67. Human Engineering Lab. http://www.dtic.mil/docs/citations/AD0666206.

Cox, H. J., and G. R. Ford. 1995. "Hearing Loss Associated with Weapons Noise Exposure: When to Investigate an Asymmetrical Loss." *The Journal of Laryngology & Otology* 109 (4): 291–95. https://doi.org/10.1017/S0022215100129950.

Dallos, Peter J. 1964. "Dynamics of the Acoustic Reflex: Phenomenological Aspects." *The Journal of the Acoustical Society of America* 36 (11): 2175–83. https://doi.org/10.1121/1.1919340.

Dancer, A., P. Grateau, A. Cabanis, J. Lejeau, and D. Lafont. 1991. "Influence of the Spacing of Impulse Noises (Weapon Noises) on the Amplitude of the TTSs in Man." *Journal d'Acoustique* 4: 421–34.

Danielson, R., D. Henderson, M. A. Gratton, L. Bianchi, and R. Salvi. 1991. "The Importance of '"Temporal Pattern"' in Traumatic Impulse Noise Exposures." *The Journal of the Acoustical Society of America* 90 (1): 209–18. https://doi.org/10.1121/1.402361.

Deiters, Kristy K., Gregory A. Flamme, Stephen M. Tasko, William J. Murphy, Nathaniel T. Greene, Heath G. Jones, and William A. Ahroon. 2019. "Generalizability of Clinically Measured Acoustic Reflexes to Brief Sounds." *The Journal of the Acoustical Society of America* 146 (5): 3993–4006. https://doi.org/10.1121/1.5132705.

DoD. 2013. “Directive 3000.03E.” USD A&S. https://www.esd.whs.mil/Portals/54/Documents/DD/issuances/dodd/300003p.pdf?ver=2018-10-24-112944-467.

Durrant, John D., and Jon K. Shallop. 1969. “Effects of Differing States of Attention on Acoustic Reflex Activity and Temporary Threshold Shift.” *The Journal of the Acoustical Society of America* 46 (4B): 907–13. https://doi.org/10.1121/1.1911809.

Engles, Warren G., Xuelin Wang, and Rong Z. Gan. 2017. “Dynamic Properties of Human Tympanic Membrane After Exposure to Blast Waves.” *Annals of Biomedical Engineering* 45 (10): 2383–94. https://doi.org/10.1007/s10439-017-1870-0.

Feeney, M. Patrick, and Chris A. Sanford. 2004. “Age Effects in the Human Middle Ear: Wideband Acoustical Measures.” *The Journal of the Acoustical Society of America* 116 (6): 3546–58. https://doi.org/10.1121/1.1808221.

Flamme, Gregory A., Kristy K. Deiters, Stephen M. Tasko, and William A. Ahroon. 2017. “Acoustic Reflexes Are Common but Not Pervasive: Evidence from the National Health and Nutrition Examination Survey, 1999–2012.” *International Journal of Audiology* 56 (sup1): 52–62. https://doi.org/10.1080/14992027.2016.1257164.

Fletcher, John L., and Arthur J. Riopelle. 1960. “Protective Effect of the Acoustic Reflex for Impulsive Noises.” *The Journal of the Acoustical Society of America* 32 (3): 401–4. https://doi.org/10.1121/1.1908079.

Greene, Nathaniel T., Mohamed A. Alhussaini, James R. Easter, Theodore F. Argo IV, Tim Walilko, and Daniel J. Tollin. 2018. “Intracochlear Pressure Measurements during Acoustic Shock Wave Exposure.” *Hearing Research* 365: 149–64. https://doi.org/10.1016/j.heares.2018.05.014.

Greene, Nathaniel T., Herman A. Jenkins, Daniel J. Tollin, and James R. Easter. 2017. “Stapes Displacement and Intracochlear Pressure in Response to Very High Level, Low Frequency Sounds.” *Hearing Research* 348: 16–30. https://doi.org/10.1016/j.heares.2017.02.002.

Gruters, Kurtis G., David L. K. Murphy, Cole D. Jenson, David W. Smith, Christopher A. Shera, and Jennifer M. Groh. 2018. “The Eardrums Move When the Eyes Move: A Multisensory Effect on the Mechanics of Hearing.” *Proceedings of the National Academy of Sciences*, E1309–18. https://doi.org/10.1073/pnas.1717948115.

JNLWP. 2015. “81 Mm Non-Lethal Indirect Fire Munition (IDFM).” Joint Non-Lethal Weapons Program. https://jnlwp.defense.gov/Portals/50/Documents/Developing_Non-Lethal_Weapons/IDFM%20Trifold_24Aug2015.pdf.

Jones, Heath G., Nathaniel T. Greene, and William A. Ahroon. 2018. “Human Middle-Ear Muscles Rarely Contract in Anticipation of Acoustic Impulses: Implications for Hearing Risk Assessments.” *Hearing Research*, December. https://doi.org/10.1016/j.heares.2018.11.006.

———. 2019. “Human Middle-Ear Muscles Rarely Contract in Anticipation of Acoustic Impulses: Implications for Hearing Risk Assessments.” *Hearing Research* 378: 53–62. https://doi.org/10.1121/1.5036449.

King, Allison, and Shelley Cazares. 2015. “Significance of Permanent Threshold Shift Potentially Caused by Sound-Based Non-Lethal Weapons.” D-5692. Institute for Defense Analyses.

Le, Trung N., Louise V. Straatman, Jane Lea, and Brian Westerberg. 2017. “Current Insights in Noise-Induced Hearing Loss: A Literature Review of the Underlying Mechanism, Pathophysiology, Asymmetry, and Management Options.” *Journal of Otolaryngology - Head & Neck Surgery* 46 (1): 41. https://doi.org/10.1186/s40463-017-0219-x.

Liang, Junfeng, Huiyang Luo, Zachary Yokell, Don U. Nakmali, Rong Zhu Gan, and Hongbing Lu. 2016. “Characterization of the Nonlinear Elastic Behavior of Chinchilla Tympanic Membrane Using Micro-Fringe Projection.” *Hearing Research* 339: 1–11. https://doi.org/10.1016/j.heares.2016.05.012.

Liang, Junfeng, Kyle D. Smith, Rong Z. Gan, and Hongbing Lu. 2019. “The Effect of Blast Overpressure on the Mechanical Properties of the Human Tympanic Membrane.” *Journal of the Mechanical Behavior of Biomedical Materials* 100 (December): 103368. https://doi.org/10.1016/j.jmbbm.2019.07.026.

Liang, Junfeng, Zachery A. Yokell, Don U. Nakmaili, Rong Z. Gan, and Hongbing Lu. 2017. “The Effect of Blast Overpressure on the Mechanical Properties of a Chinchilla Tympanic Membrane.” *Hearing Research* 354: 48–55. https://doi.org/10.1016/j.heares.2017.08.003.

Loeb, M., J. L. Fletcher, and R. W. Benson. 1965. “Some Preliminary Studies of Temporary Threshold Shift with an Arc-Discharge Impulse-Noise Generator.” *The Journal of the Acoustical Society of America* 37 (2): 313–18. https://doi.org/10.1121/1.1909328.

Loeb, Michel, and John L. Fletcher. 1968. “Impulse Duration and Temporary Threshold Shift.” *The Journal of the Acoustical Society of America* 44 (6): 1524–28. https://doi.org/10.1121/1.1911291.

McGregor, Kara D., Gregory A. Flamme, Stephen M. Tasko, Kristy K. Deiters, William A. Ahroon, Christa L. Themann, and William J. Murphy. 2018. “Acoustic Reflexes Are Common but Not Pervasive: Evidence Using a Diagnostic Middle Ear Analyser.” *International Journal of Audiology* 57 (sup1): S42–50. https://doi.org/10.1080/14992027.2017.1416189.

Munjal, K. R., and Major V. P. Singh. 1997. “Impulse Noise Trauma during Army Weapon Firing | SpringerLink.” *IJO & HNS* 49. https://link.springer.com/article/10.1007/BF03023801.

Nageris, Ben I., Eyal Raveh, Michal Zilberberg, and Joseph Attias. 2007. “Asymmetry in Noise-Induced Hearing Loss: Relevance of Acoustic Reflex and Left or Right Handedness.” *Otology & Neurotology* 28 (4): 434. https://doi.org/10.1097/mao.0b013e3180430191.

Patterson, James H., Jr., Ben T. Mozo, Elmaree Gordon, Jesus R. Canales, and Daniel L. Johnson. 1997. “Pressures Measured under Earmuffs Worn by Human Volunteers during Exposure to Freefield Blast Overpressures.” USAARL 98-01. U.S. Army Aeromedical Research Laboratory.

Pfander, F., H. Bongartz, H. Brinkmann, and H. Kietz. 1980. “Danger of Auditory Impairment from Impulse Noise: A Comparative Study of the CHABA Damage-risk Criteria and Those of the Federal Republic of Germany.” *The Journal of the Acoustical Society of America* 67 (2): 628–33. https://doi.org/10.1121/1.383886.

Smoorenburg, G. F. 2003. “Reconsideration of the Effects of Impulse Noise.” RTO Technical Report RTO TR-017. North Atlantic Treaty Organisation.

Swallow, Jessica G., and Corinne M. Kramer. 2019. “Uncertainty of Auditory Injury Models for Flashbangs.” D-10722. Institute for Defense Analyses.

Swallow, Jessica G., and Felicia D. Sallis-Peterson. 2020. “Assessment of the Tympanic Membrane Rupture Model for Predicting Injury Risk of Flashbangs.” D-13104. Institute for Defense Analyses.

Wang, Hongyun, Wesley A. Burgei, and Hong Zhou. 2017. “Interpreting Dose-Response Relation for Exposure to Multiple Sound Impulses in the Framework of Immunity.” *Health* 09 (13): 1817. https://doi.org/10.4236/health.2017.913132.

———. 2018. “Risk of Hearing Loss Injury Caused by Multiple Flash Bangs on a Crowd.” *American Journal of Operations Research* 08 (04): 239. https://doi.org/10.4236/ajor.2018.84014.

REPORT DOCUMENTATION PAGE

Form Approved
OMB No. 0704-0188

The public reporting burden for this collection of information is estimated to average 1 hour per response, including the time for reviewing instructions, searching existing data sources, gathering and maintaining the data needed, and completing and reviewing the collection of information. Send comments regarding this burden estimate or any other aspect of this collection of information, including suggestions for reducing the burden, to Department of Defense, Washington Headquarters Services, Directorate for Information Operations and Reports (0704-0188), 1215 Jefferson Davis Highway, Suite 1204, Arlington, VA 22202-4302. Respondents should be aware that notwithstanding any other provision of law, no person shall be subject to any penalty for failing to comply with a collection of information if it does not display a currently valid OMB control number.

PLEASE DO NOT RETURN YOUR FORM TO THE ABOVE ADDRESS.

1. REPORT DATE	2. REPORT TYPE	3. DATES COVERED *(From–To)*
March 2021	FINAL	

4. TITLE AND SUBTITLE

Risk of Auditory Injury Caused by Area-Effect Flashbangs: Multiple Area-Distributed Impulses and the Role of the Acoustic Reflex

5a. CONTRACT NUMBER
HQ0034-14-D-0001

5b. GRANT NUMBER

5c. PROGRAM ELEMENT NUMBER

6. AUTHOR(S)

Swallow, Jessica G.
Fedele, Emily A.
Sallis-Peterson, Felicia D.

5d. PROJECT NUMBER
DU-2-4640

5e. TASK NUMBER

5f. WORK UNIT NUMBER

7. PERFORMING ORGANIZATION NAME(S) AND ADDRESS(ES)

Institute for Defense Analyses
Systems and Analyses Center
4850 Mark Center Drive
Alexandria, VA 22311-1882

8. PERFORMING ORGANIZATION REPORT NUMBER

IDA Document D-21609

9. SPONSORING / MONITORING AGENCY NAME(S) AND ADDRESS(ES)

Joint Intermediate Force Capabilities Office
3097 Range Road
Quantico, VA 22134

10. SPONSOR/MONITOR'S ACRONYM(S)

JIFCO

11. SPONSOR/MONITOR'S REPORT NUMBER(S)

12. DISTRIBUTION/AVAILABILITY STATEMENT

Approved for public release; distribution is unlimited (10 June 2021).

13. SUPPLEMENTARY NOTES

14. ABSTRACT

Human effects modeling of intermediate force capabilities includes the goal of estimating the risk of injury associated with devices that are used in highly variable operational settings. In the case of multi-impulse flashbangs, existing models for risk of hearing loss do not typically capture the uncertainties associated with the timing and spatial distribution of multiple impulses. Existing models also do not accurately model the effect of the acoustic reflex, which should be activated for a short time after a loud impulse noise exposure in some fraction of the population. In lieu of accurate modeling of these types of effects (timing, distribution, and physiological), the expected injury risk can be bounded by applying limiting assumptions on dose accumulation. In this report, we apply this bounding approach to estimate the risk of hearing loss for multi-impulse, area-distributed sound exposure scenarios. Using Monte-Carlo simulations, we also explore the role of variables such as the number of impulses, their spatial distribution, and the uncertainty in individual impulse intensity on the expected risk of injury. We show that the uncertainty in the estimate of injury risk is greater for more intense exposures or those with more impulses, and demonstrate the importance of accounting for sound output variation and multi-impulse distribution in mapping risk of injury within an area.

15. SUBJECT TERMS

flashbang; impulse noise; Non-Lethal Weapon (NLW); permanent threshold shift (PTS); Risk of Significant Injury (RSI)

16. SECURITY CLASSIFICATION OF:			17. LIMITATION OF ABSTRACT	18. NUMBER OF PAGES	19a. NAME OF RESPONSIBLE PERSON
					Burgei, Wesley
a. REPORT Uncl.	b. ABSTRACT Uncl.	c. THIS PAGE Uncl.	SAR	67	19b. TELEPHONE NUMBER *(include area code)* 703-432-0899

Standard Form 298 (Rev. 8-98)
Prescribed by ANSI Std. Z39.18